9

Research Article

Lingyu Li, Hongkang Chen*, Hongfa Yu*, Haiyan Ma*, Haotian Fan, Xiaoqing Chen, and Yuning Gao

A sawtooth constitutive model describing strain hardening and multiple cracking of ECC under uniaxial tension

https://doi.org/10.1515/rams-2024-0048 received June 10, 2023; accepted July 10, 2024

Abstract: By collecting engineered cementitious composite (ECC) uniaxial tensile experimental research data, aiming at the multiple cracking characteristics of the strain hardening stage of the ECC stress-strain curve, a theoretical model describing the constitutive relationship of the ECC uniaxial tensile stress-strain - the multiple cracking sawtooth model – is proposed. Several model parameters were obtained with the fitting analysis of many ECC uniaxial tensile stress-strain curves. The application conditions and influencing factors of the three-order multi-crack "sawtooth" model of polyvinyl alcohol (PVA)-ECC and polyethylene (PE)-ECC and the four-order multi-crack "sawtooth" model of PVA-ECC are studied. The result shows that the higher the fiber reinforcement index, the better the tensile properties of ECC. The fiber reinforcement index is linearly correlated with the initial crack stress and ultimate tensile stress of PVA-ECC and with the ultimate tensile stress and ultimate tensile strain of PE-ECC. The characteristic points of PVA-ECC in the multi-crack cracking stage are as follows: the greater the initial cracking strain, the smaller the ultimate tensile strain, showing an exponential correlation; The greater the initial cracking stress is, the greater the ultimate tensile stress is, and the two are linearly correlated.

Keywords: engineered cementitious composites, strain hardening, multiple cracking constitutive model, stress–strain curve

1 Introduction

Li and Leung [1,2] first proposed the basic design concept of engineered cementitious composite (ECC) using micromechanics and fracture mechanics as the basic principles. ECC are materials with ductility and tensile strain capacity, generally more than 3% [3–5]. Over the years, Li's team has conducted much research on ECC's processing [6–8], mechanical properties [9–11], durability [12–15], etc., with outstanding results. ECCs' application prospects are broad; they have been used to repair concrete structures [16], to build link slabs for bridge decks [17,18], as well as other projects [19–23].

ECC is an extraordinary example of concrete material design based on mechanical principles. Making full use of multiple cracking, ECC obtains a cement-based composite material similar to the strain-hardening behavior of metal materials, as shown in Figure 1 [24]. It subverts the brittle characteristics of the mechanical properties of traditional cement concrete.

Aveston and Kelly [25] has made pioneering research on the phenomenon of multiple cracking in fiber-reinforced cementitious composites, and it is pointed out that when the matrix of continuous fiber-reinforced composite fails under lower strain than that of fiber, the matrix will crack many times as long as the fiber tensile property is strong enough to bear the additional load. Now, scholars use the micromechanics method [26–28], discrete element method [29–32], and finite element method [33] to establish different models to describe the tensile behavior of ECCs. Besides, there is also the use of mathematical methods to describe the ECC uniaxial tensile stress–strain relationship. Li [34] proposed a three-linear model of the ECC uniaxial tensile stress–strain curve, as shown in Figure 2a. In stage I, ECC is linear elastic deformation, no cracks appear, and

^{*} Corresponding author: Hongkang Chen, Department of Civil Engineering, College of Civil Aviation, Nanjing University of Aeronautics and Astronautics, Nanjing, 211100, China, e-mail: chrisprism1997@outlook.com

^{*} Corresponding author: Hongfa Yu, Department of Civil Engineering, College of Civil Aviation, Nanjing University of Aeronautics and Astronautics, Nanjing, 211100, China, e-mail: yuhongfa@nuaa.edu.cn

^{*} Corresponding author: Haiyan Ma, Department of Civil Engineering, College of Civil Aviation, Nanjing University of Aeronautics and Astronautics, Nanjing, 211100, China, e-mail: mahaiyan@nuaa.edu.cn Lingyu Li, Haotian Fan, Xiaoqing Chen, Yuning Gao: Department of Civil Engineering, College of Civil Aviation, Nanjing University of Aeronautics and Astronautics, Nanjing, 211100, China

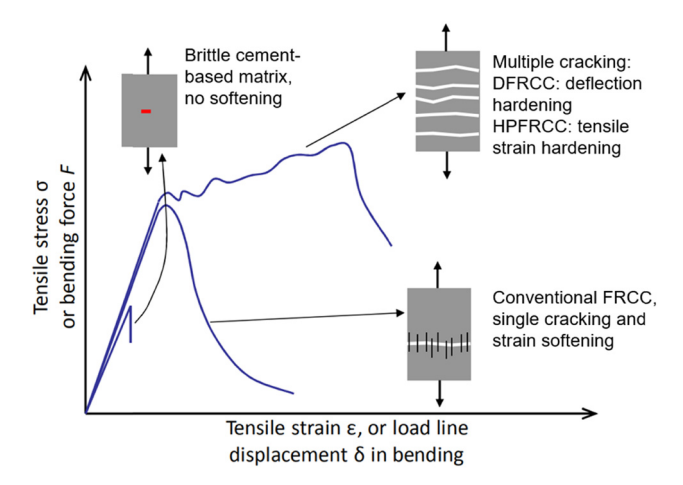


Figure 1: Comparison of uniaxial tensile stress–strain curves of ECC, brittle cement-based matrix, and conventional FRCC [24].

the end of this stage is before the first crack appears. Stage II and stage III are multiple cracking stages, the slopes of the two stages are different, and the end of the multiple cracking stages is when the ultimate stress is reached. Kanda *et al.* [35] proposed a bilinear uniaxial tensile constitutive model. Moreover, based on the bilinear model, Guo *et al.* [16] proposed a new bilinear constitutive equation for ECC uniaxial tension using the nominal initial crack stress point and the nominal maximum tensile stress point as the control points. This overcomes the problem of excessive or insufficient margin when calculating the bearing capacity of the classic bilinear model.

Muhammer *et al.* [36] studied the effects of W/B ratio and mineral additives on the fiber-matrix synergy in polyvinyl alcohol (PVA)-ECC, Tawfek *et al.* [37] studied the effects of fiber orientation and distribution on the mechanical properties of ECC, and Do *et al.* [38] discussed the potential of ECC to replace cement mortar in traditional iron cement. Mahmoudi *et al.* [39] studied polyethylene (PE)-ECC specimens' residual compression and tensile properties after

exposure under high-temperature conditions. In the above research process, it is found that the stress–strain curves of ECC show the characteristics of strain hardening under uniaxial tension.

Wu et al. [40] conducted uniaxial tensile tests on Ultra-High Strength and High Ductility Cementitious Composite (UHS-HDCC) specimens to evaluate the strain hardening properties of UHS-HDCC. The results show that all UHS-HDCC specimens exhibit significant strain-hardening behavior after initial cracking, accompanied by multiple cracks. With the increase of GGBS content and the decrease of SF content, the degree of saturated cracking of UHS-HDCC increases. Figure 3 shows the tensile stress–strain curve and crack cracking mode of UHS-HDCC with 30% GGBS and 10% SF. It can be observed from the diagram that a large number of saturated and approximately parallel cracks are generated in the tensile area of the sample.

Wu *et al.* [41] studied the tensile stress–strain curves and multiple cracking characteristics of UHS-HDCCs incorporating pure ultra-high molecular weight PE fiber and modified behavior and remarkable tensile strain capacity. The crack pattern of fibers when subjected to increasing tensile load is illustrated in Figure 4. It is found that all UHS-HDCC mixtures exhibit strain hardening. The dog-bone specimen is marked by multiple narrow cracks observed in the tensile region.

This article presents a mathematics-based sawtooth constitutive model to capture the variability of the tensile behavior of ECCs. In the strain hardening section, a sawtooth wave function and a piecewise function are superimposed to form a new function to represent the fluctuation of the sawtooth section of the strain hardening section. The model is validated by comparing it with experimental results. The constitutive relation of ECC tensile properties was studied by fitting the model parameters. In addition, the characteristic points in the stress–strain curve representing the beginning of the strain-hardening stage are analyzed.

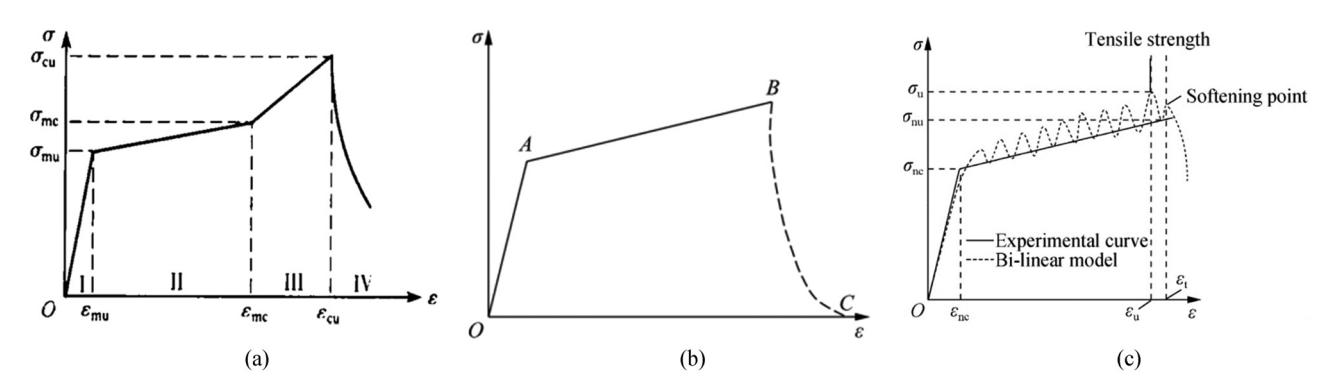


Figure 2: Constitutive model to describe ECC tensile behavior: (a) three-linear model [34], (b) classic bilinear model [35], and (c) bilinear model [16].

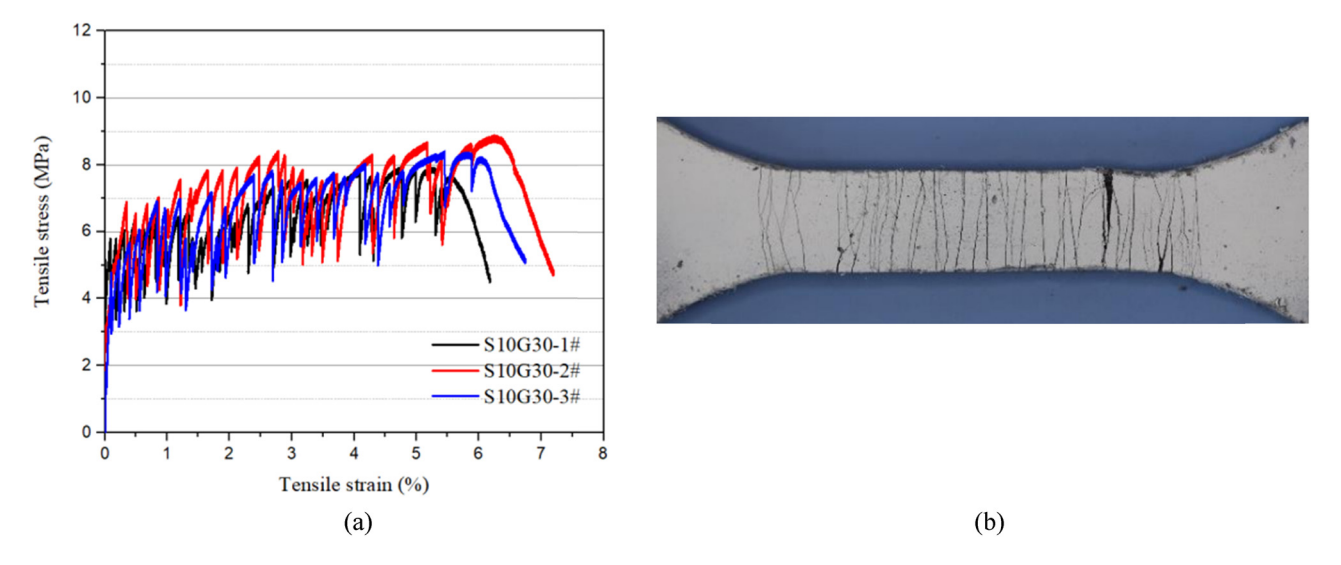


Figure 3: The tensile stress-strain curve and crack cracking mode of UHS-HDCC (\$10G30) [40]: (a) the tensile stress-strain curves of UHS-HDCC (S10G30), (b) the crack pattern of UHS-HDCC tensile plane (S10G30).

On September 10, 2023, in the Elsevier library database, the keyword ECC was entered in the Find articles with terms, and 37,868 scientific literature about ECC was retrieved. In the first 10 SCI articles [42-51], ECC tensile stress-strain curves align with the sawtooth model. For example, selecting the literature [42,44,46,50] randomly, it can be seen from Figure 6 that its ECC tensile stress-strain curves are all sawtooth, where Figure 6(a) is Figure 8(h) of ref. [42], Figure 6(b) is Figure 5(a) of ref. [44], Figure 6(c) is the third graph of Figure 8 of ref. [46], and Figure 6(d) is Figure 3 of ref. [50], which is enough to prove that the mathematical model of the tensile stress-strain curve of the ECC material can be summarized into the sawtooth model.

2 Modeling approach

2.1 Multiple cracking sawtooth model

In ECC's multiple cracking models, there are many "saw teeth" in the strain-hardened section. Generating serrations is an essential feature of multiple cracking: cracking includes the appearance of new cracks and the expansion of existing cracks. Many literature data charts show that the number of early teeth is often higher in the strain hardening section, and the growth rate is faster. While the later period is less, the growth rate is slower, and even negative growth may occur, so the strain hardening

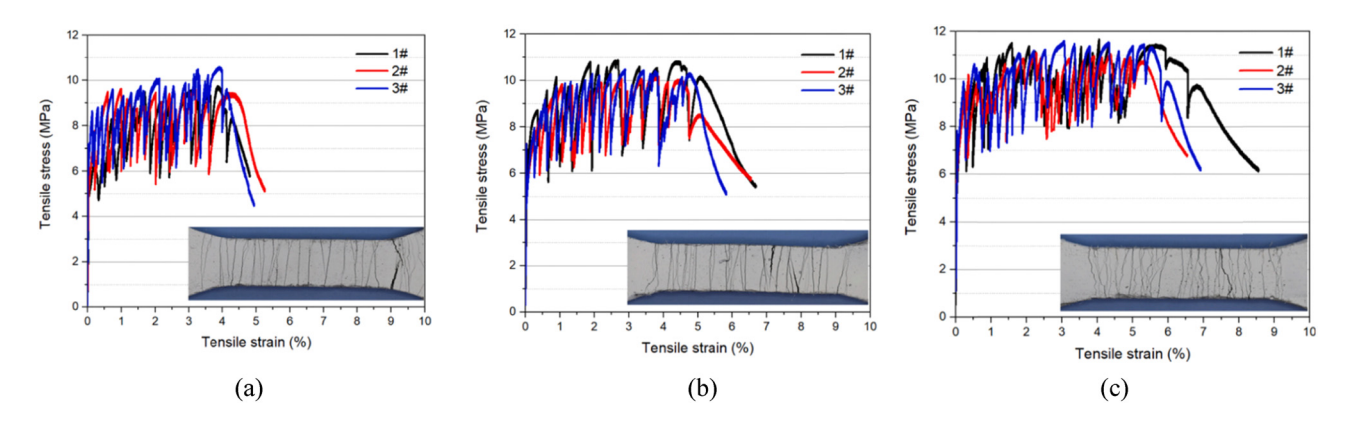


Figure 4: The tensile stress-strain curves and multiple cracking characteristics of UHS-HDCCs with pristine PE fibers and modified fibers [41]: (a) pristine PE fiber, (b) PDA-PE fiber, and (c) SiO₂-PDA-PE fiber.



Figure 5: ECC-related literature search results.

section model should be established in two segments, as (1) The stress-strain curve of ECC uniaxial tension is shown in Figure 7a.

There are two assumptions:

assumed to be linearly elastic before the first crack occurs before the stress reaches the initial cracking

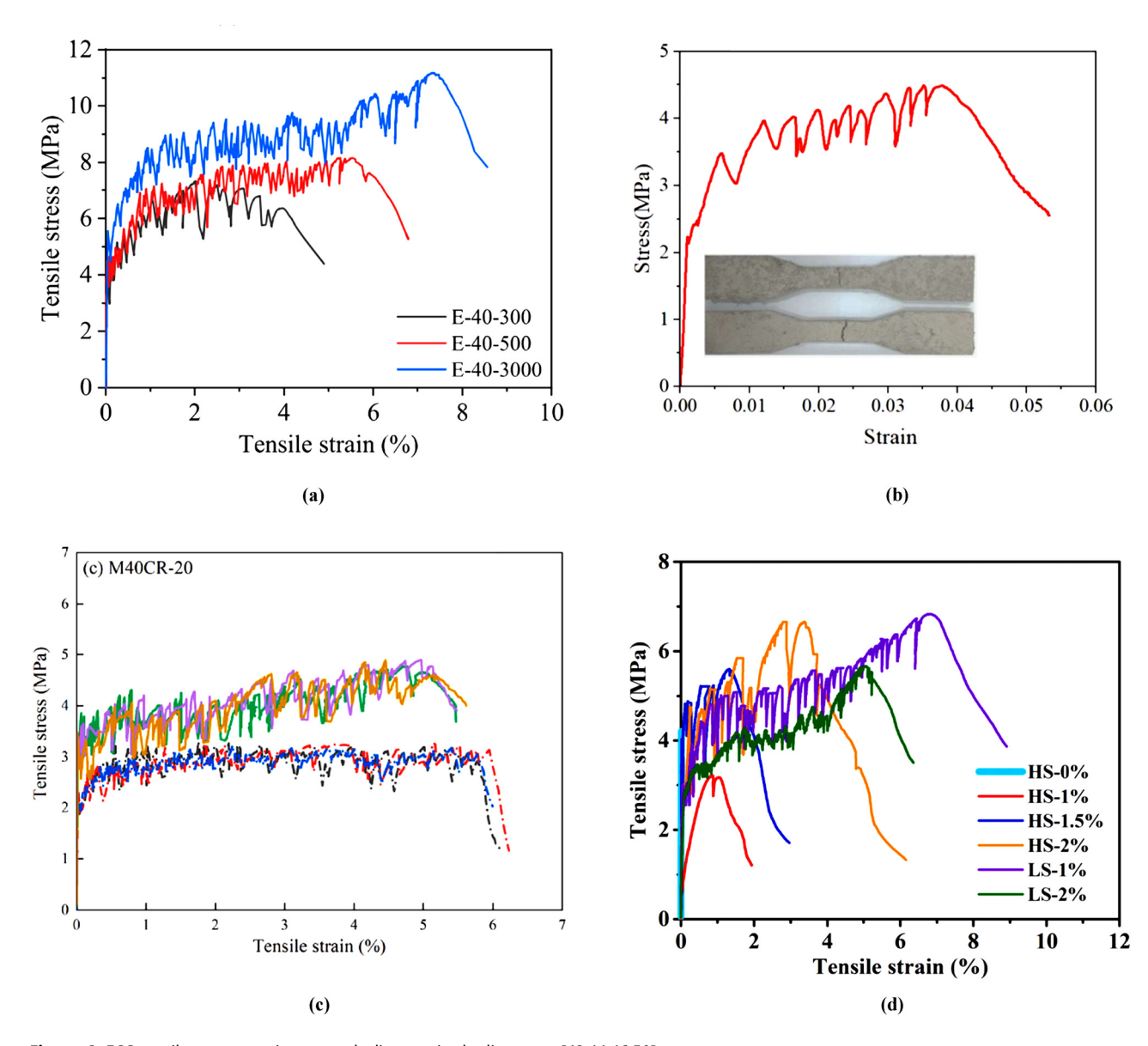


Figure 6: ECC tensile stress-strain sawtooth diagram in the literature [42,44,46,50].

stress. The curve in the first stage only needs to establish the relationship between the elastic modulus E_c and the cracking stress.

(2) The strain hardening stage is assumed to be a sawtooth period function A whose peak value will change. The function formula is:

$$A = \left(-\frac{2}{\pi}\right) \times \sum \frac{\sin(2\pi k f \varepsilon)}{k} (k = 1, 2, 3, \dots \infty).$$
 (1)

According to the above model and mechanical principle, the constitutive equation is as follows:

$$\sigma(\varepsilon) = E_{\rm c}\varepsilon, \, \varepsilon \le \varepsilon_{\rm fc}, \tag{2}$$

$$\sigma(\varepsilon) = \sigma_{\rm fc} + \frac{A_1}{a_1} + b_1(\varepsilon - \varepsilon_{\rm fc}), \, \varepsilon_{\rm fc} < \varepsilon < \varepsilon_1, \tag{3}$$

$$\sigma(\varepsilon) = \sigma_{fc} + \frac{A_1}{a_1} + b_1(\varepsilon - \varepsilon_{fc}), \, \varepsilon_{fc} < \varepsilon < \varepsilon_1,$$

$$\sigma(\varepsilon) = \sigma_1 + \frac{A_2}{a_2} + b_2(\varepsilon - \varepsilon_1), \, \varepsilon_1 \le \varepsilon \le \varepsilon_u,$$
(4)

$$\sigma(\varepsilon) = \sigma_{\rm u} \frac{\frac{\varepsilon}{\varepsilon_{\rm u}}}{c \left(\frac{\varepsilon}{\varepsilon_{\rm u}} - 1\right)^2 + \frac{\varepsilon}{\varepsilon_{\rm u}}}, \, \varepsilon_{\rm u} < \varepsilon < \varepsilon_{\rm nu}.$$
 (5)

Among them, A_1 and A_2 are sawtooth wave functions, and parameters a, b, c, and f are related to the fiber volume dosage, fiber type, and the mixing ratio of the matrix material. $\varepsilon_{\rm fc} < \varepsilon_1 \le \varepsilon_0$, ε_0 is the strain when the composite material reaches the ultimate tensile stress.

$$A_1 = \left(-\frac{2}{\pi}\right) \times \sum \frac{\sin(2\pi k f_1(\varepsilon - \varepsilon_{\rm fc}))}{k} (k = 1, 2, 3, \dots \infty), \quad (6)$$

$$A_2 = \left(-\frac{2}{\pi}\right) \times \sum \frac{\sin(2\pi k f_2(\varepsilon - \varepsilon_1))}{k} (k = 1, 2, 3, \dots \infty). \tag{7}$$

 $\sigma_{\rm fc}$ and $\sigma_{\rm u}$, respectively, refer to the initial cracking stress, the stress at the end of the hardened section I, and the ultimate tensile stress. $\varepsilon_{\rm fc}$, $\varepsilon_{\rm l}$, $\varepsilon_{\rm u}$ and $\varepsilon_{\rm nu}$ refer to the initial cracking strain, the strain at the end of the hardened section I, the strain when the ultimate tensile stress is reached, and the ultimate strain, respectively.

Parameter a determines the difference between the peaks and valleys of the sawtooth section function (referred to as the amplitude), and b is related to the difference between the segmental stress in the sawtooth segment and the difference between the peaks and valleys and the segment length. The formulas are shown in (8) and (9):

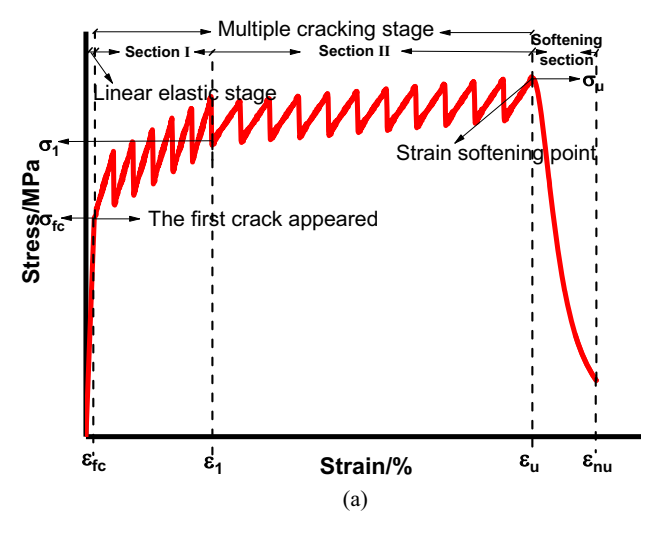
$$b_1 = \frac{\sigma_1 - \sigma_{fc} - \frac{1}{a}}{\varepsilon_1 - \varepsilon_{fc}},\tag{8}$$

$$b_2 = \frac{\sigma_{\rm u} - \sigma_1 - \frac{1}{a}}{\varepsilon_{\rm u} - \varepsilon_1}.$$
 (9)

The strain softening section refers to the descending section formula of the concrete uniaxial compressive stressstrain curve. The parameter c is proposed. The smaller the parameter c value, the smoother the strain softening section, indicating the better the material's ductility. Here, f represents the frequency of the sawtooth in the strain-hardening section. The larger the f, the denser the sawtooth, and *vice* versa, the sparser sawtooth.

Parameter d represents the strain hardening section I proportion in multiple cracking stages. This parameter is related to calculating the relative stress increments of the two hardening sections. The relationship is:

$$\Delta_1 = \frac{1}{a_1'} + b_1' \times d \times (\varepsilon_{\rm u} - \varepsilon_{\rm fc}), \tag{10}$$



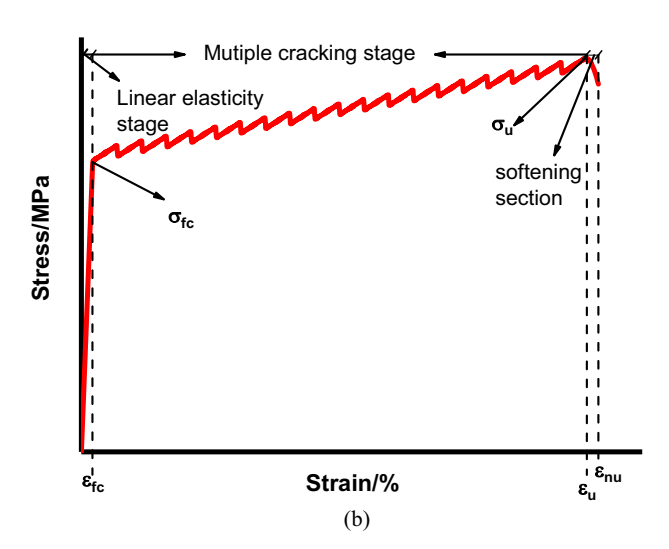


Figure 7: Multiple cracking sawtooth model: (a) four-segment (two-segment hardening), (b) three-segment (one-segment hardening).

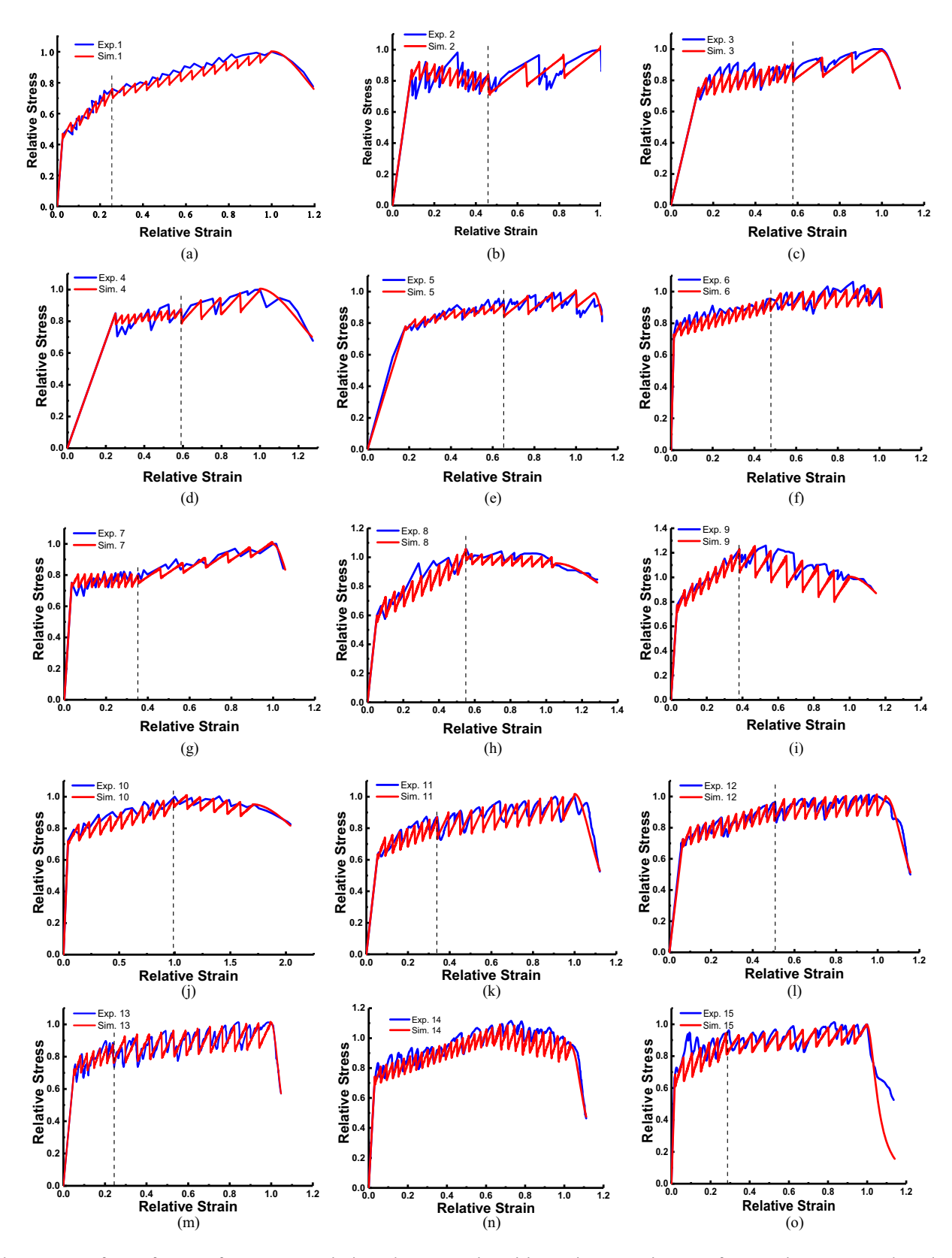


Figure 8: Curve fitting of PVA-ECC four-segment multiple cracking sawtooth model: (a) 1, (b) 2, (c) 3, (d) 4, (e) 5, (f) 6, (g) 7, (h) 8, (i) 9, (j) 10, (k) 11, (l) 12, (m) 13, (n) 14, and (o) 15.

$$\Delta_2 = \frac{1}{a_2'} - \frac{1}{a_1'} + b_1' \times (1 - d) \times (\varepsilon_{\mathrm{u}} - \varepsilon_{\mathrm{fc}}), \tag{11}$$

$$\Delta_1 + \Delta_2 + \frac{\sigma_{\rm fc}}{\sigma_{\rm u}} = 1. \tag{12}$$

When $a_1 = a_2 = a$, $b_1 = b_2 = b$, and $f_1 = f_2$ are in the fourstage multiple cracking sawtooth model, a three-segment multiple cracking sawtooth model will appear. The linear elastic stage and strain softening stage of the three-segment multiple sawtooth model are consistent with the first and fourth segments of the four-segment multiple sawtooth models, as shown in Figure 5b. Among them, σ_{fc} and $\sigma_{\rm u}$ refer to initial cracking stress and ultimate tensile stress, respectively. ε_{fc} , ε_{u} , and ε_{nu} refer to the initial cracking strain, the strain when the ultimate tensile stress is reached, and the ultimate strain, respectively. At this time, for this particular situation, set f = 20, the hardening section has only two undetermined parameters, a and b, and the following relationships exist:

$$\frac{-\frac{2}{\pi}\sum_{k}\frac{\sin(2\pi kf(\varepsilon-\varepsilon_{\text{fc}}))}{k}(k=1,2,\cdots,\infty)}{a} \in \left[-\frac{1}{a}, \frac{1}{a}\right], \quad (13)$$

$$b = \frac{\sigma_{\rm u} - \sigma_{\rm fc} - \frac{1}{a}}{\varepsilon_{\rm u} - \varepsilon_{\rm fc}} \tag{14}$$

According to the above model and mechanics principle, the constitutive relationship is as follows:

$$\sigma(\varepsilon) = E_{\rm c}\varepsilon, \, \varepsilon \le \varepsilon_{\rm fc}, \tag{15}$$

$$\sigma(\varepsilon) = \sigma_1 + \frac{A}{a} + b(\varepsilon - \varepsilon_1), \, \varepsilon_{fc} \le \varepsilon \le \varepsilon_{u}, \tag{16}$$

$$\sigma(\varepsilon) = \sigma_{1} + \frac{A}{a} + b(\varepsilon - \varepsilon_{1}), \, \varepsilon_{fc} \le \varepsilon \le \varepsilon_{u}, \qquad (16)$$

$$\sigma(\varepsilon) = \sigma_{u} \frac{\frac{\varepsilon}{\varepsilon_{u}}}{c\left(\frac{\varepsilon}{\varepsilon_{u}} - 1\right)^{2} + \frac{\varepsilon}{\varepsilon_{u}}}, \, \varepsilon_{u} < \varepsilon < \varepsilon_{nu}. \qquad (17)$$

2.2 Model data collection

In order to make the theoretical model of the ECC uniaxial tensile stress-strain curve universal, this article randomly collects dozens of domestic and foreign literature on the tensile properties of high ductility cement-based composites for research. In the PVA-ECC literature, the raw materials, mix ratio, and other conditions are as follows:

- (1) The cement is P.O 42.5R or P.O 52.5R, the fine aggregate is fine sand, the filler is grade I fly ash, and the waterreducing agent is polycarboxylate superplasticizer.
- (2) The water-binder ratio is mainly between 0.27 and 0.38, and the cement-sand ratio is mainly between 1:0.8 and 3:0.35. The fly ash content is 0, 5, 10, 50, 60, 70, 75, and 80%.

(3) The mechanical indexes of the starting point of multi-crack cracking of composite materials are initial crack strain range: 0.05-0.55%, initial crack stress range: 1.41-4.68 MPa, ultimate tensile strain range: 0.51-7.17%, and ultimate tensile stress range: 1.86-5.82 MPa.

In the PE-ECC literature, raw materials, mix ratio, and other conditions are as follows:

- (1) Cement is P.O 42.5R or P.O 52.5R, fine aggregate is fine sand, the filler is a grade I fly ash, slag, limestone, or silica fume, and water reducer is polycarboxylate superplasticizer.
- (2) The water-binder ratio is concentrated between 0.135 and 0.32, the ash-sand ratio is concentrated between 2:1 and 1.5:1, the fly ash content is between 0 and 10%, the slag content is 0 or 50%, the silica fume content is 0 or 10%, and the limestone content is 0-6%.
- (3) The mechanical indexes of the initiation point of multicrack cracking of composite materials are as follows: initial crack strain range: 0.12-0.46%, initial crack stress range: 1.53–12.09 MPa, ultimate tensile strain range: 2.20–13.32%, and ultimate tensile stress range: 3.58-17.75 MPa.

2.3 Model data processing and induction

The "normalization method" analyzes multiple fitting parameters and establishes ECC's tensile stress-strain constitutive relationship. Establish a relative stress-relative strain curve; the relative stress is equal to the ratio of the stress to the maximum stress, and the relative strain is equal to the ratio of the strain to the strain when the specimen reaches the maximum stress. The relevant parameters are adjusted to:

$$a' = a \times \sigma_{\rm u}, \tag{18}$$

$$b' = \frac{b}{\sigma_{v}},\tag{19}$$

$$f' = f \times \varepsilon_{11}. \tag{20}$$

The method of multi-factor combination is used to study the factors that affect ECC tensile performance indicators. Combining fiber type, aspect ratio, and fiber content and exploring whether it has a constitutive relationship with ECC's initial cracking stress, initial cracking strain, ultimate tensile stress, and ultimate tensile strain. If it exists, explore whether the parameters of the constitutive equation have a clear mechanical meaning. In addition, through a large amount of experimental data, it is explored whether there is an inherent relationship between the initial cracking stress, initial cracking strain, ultimate tensile stress, and ultimate tensile strain of ECC. If it exists, put forward the constitutive equation.

3 PVA-ECC uniaxial tensile stress-strain constitutive relationship

3.1 Four-segment multiple cracking sawtooth model fitting and parameter law

Five articles [16,52–55] with similar matrix material ratios were selected for the four-segment multiple cracking sawtooth model for fitting analysis. The fitting situation is shown in Figure 8.

The fitting parameters are shown in Table 1. Among the 15 data, there are 11 data where a_1' is more significant than a_2' ; that is, the difference between the peaks and valleys of the early sawtooth section in the PVA-ECC uniaxial tensile stress–strain curve is smaller than the difference between the peaks and valleys of the late sawtooth section. The value of a_1' is concentrated between 17 and 35, and the value of a_2' is concentrated between 12 and 31. In 12 data, b_1' is more significant than b_2' , and in 3 data, b_1' is less than b_2' . The value of b_1' is concentrated between 0 and 0.25, and the value of b_2' is concentrated between -0.09 and 0.14. The value of d is concentrated between 0.3 and 0.6.

These three parameters work together to express the increase of the hardened segment. The three parameters have a more extensive range, so the three parameters are considered together. In the three data, the stress increment Δ_{II} of hardening section I is smaller than the stress increment Δ_{II} of hardening section II. When the four-segment multiple cracking sawtooth model is used to fit the PVA-ECC uniaxial

tensile stress–strain curve, the stress increment of hardened section I is often more significant than that of hardened section II. In addition, four sets of data have a negative Δ_{II} . PVA-ECC with high fly ash content reaches the ultimate tensile stress earlier in uniaxial tension, but it can still maintain a higher stress level in a more extended strain change.

In 15 data sets, f_1' is more significant than f_2' in all the group segments. It expresses that the sawtooth segment is denser in the early stage and sparser in the later stage. The value of f_1' is concentrated between 20 and 32, and the value of f_2' is concentrated between 5.5 and 20.

In summary, using the four-segment multiple cracking sawtooth model to fit the PVA-ECC uniaxial tensile stress—strain curve, it can be found that the overall stress of hardened section I increases more, and the sawtooth is denser. In contrast, the overall stress of hardened section II increases less and more sparse and jagged.

3.2 Three-segment multiple cracking sawtooth model fitting and parameter law

Four articles [53,56–58] with similar matrix material ratios were selected for the three-segment multiple cracking sawtooth model for fitting analysis. The fitting situation is shown in Figure 9.

The fitting parameters are shown in Table 2. In the curve fitted by the three-segment multiple cracking sawtooth model, the value of a' is concentrated between 20 and 45. This is larger than a_1' and a_2' in the four-segment multiple cracking model. It

		_		_		
Table 1: Fitting	narameters of	PVA-FCC uni	iavial tension	four-seament	multiple sa	awtooth model

	V _f (%)	FA (%)	a_1'	a_2'	b_1'	b ' ₂	c'	d	f_1'	f_2'	Δı	Δ _{II}
1 [52]	1	0	29.11	34.93	1.54	0.46	10	0.238	25.83	18.7	0.302	0.247
2 [53]	1.5	0	17.86	14.89	-0.11	0.14	30	0.405	27.17	5.56	-0.03	0.167
3	1.5	0	18.01	17.83	0.11	0.10	44	0.514	26.87	7.10	0.159	0.089
4	1.5	10	35.52	17.76	0.00	0.24	7	0.454	29.37	9.78	0.028	0.121
5	1.5	10	38.69	19.35	0.25	0.12	150	0.575	21.26	8.63	0.190	0.083
6 [54]	1.5	75	23.14	18.51	0.07	0.01	1,000	0.468	30.34	19.08	0.203	0.045
7	1.5	75	23.48	31.31	0.01	0.07	60	0.332	31.27	9.30	0.056	0.190
8 [55]	1.7	50	14.44	28.88	0.23	-0.01	4	0.528	19.99	13.43	0.457	-0.056
9	1.7	70	17.12	10.06	0.21	-0.09	6	0.361	20.91	13.33	0.446	-0.228
10	1.7	80	19.60	23.52	0.11	-0.04	5	0.571	10.43	8.33	0.274	-0.054
11 [16]	2	60	14.31	14.15	0.28	0.09	70	0.302	28.04	18.19	0.237	0.129
12	2	60	17.09	14.95	0.11	0.02	85	0.470	27.29	20.21	0.243	0.046
13	2	60	17.96	12.83	0.10	0.03	350	0.198	31.88	17.10	0.152	0.122
14	2	60	18.34	12.84	0.12	-0.07	190	0.621	33.27	27.25	0.326	-0.071
15	2	60	13.34	17.78	0.27	0.04	300	0.267	22.87	15.30	0.260	0.055

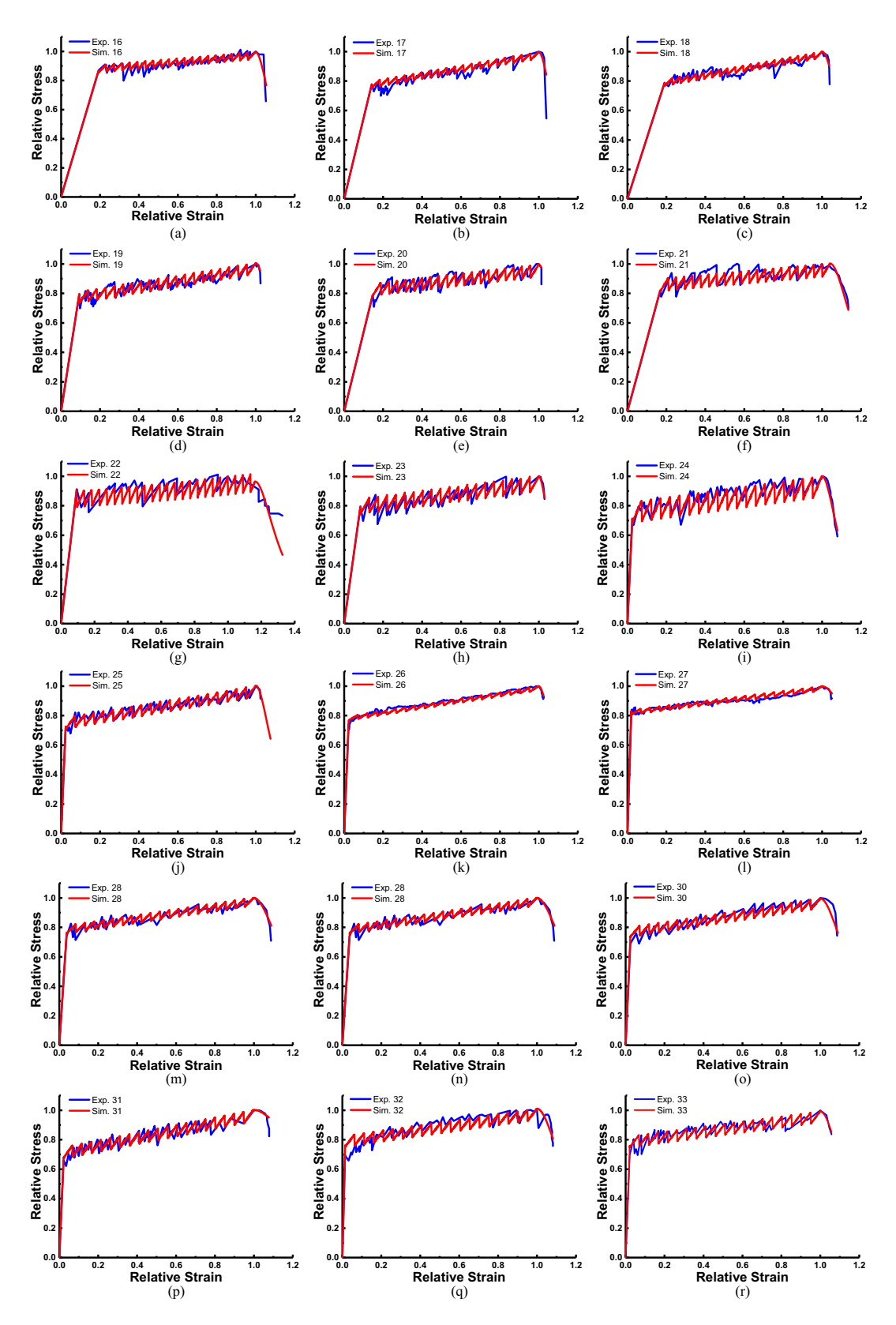


Figure 9: Curve fitting of PVA-ECC three-segment multiple cracking sawtooth model: (a) 16, (b) 17, (c) 18, (d) 19, (e) 20, (f) 21, (g) 22, (h) 23, (i) 24, (j) 25, (k) 26, (l) 27, (m) 28, (n) 29, (o) 30, (p) 31, (q) 32, and (r) 33.

Table 2: Fitting parameters of PVA-ECC uniaxial tension three-segment multiple sawtooth model

	V _f (%)	FA (%)	a'	b'	c'	f ′	Δ
16 [53]	1.75	10	39.45	0.06	100	24.78	0.085
17	1.75	10	43.84	0.09	120	23.30	0.127
18	1.75	10	45.26	0.10	80	24.71	0.217
19	1.75	5	25.91	0.11	100	22.04	0.099
20	1.75	5	23.49	0.12	105	23.44	0.137
21	1.75	5	24.14	0.11	80	24.06	0.143
22	1.75	0	17.07	0.02	60	22.07	0.191
23	1.75	0	20.19	0.07	190	21.82	0.262
24 [56]	2	10	23.40	80.0	100	20.51	0.341
25	2	10	25.58	0.07	105	20.48	0.317
26 [57]	2	5	70.40	0.04	115	20.45	0.278
27	2	5	63.32	0.02	40	20.40	0.177
28 [58]	2	0	36.74	0.07	30	20.76	0.269
29	2	0	33.57	0.08	30	20.37	0.386
30	2	0	30.43	0.09	40	20.48	0.310
31	2	0	25.95	80.0	9	20.45	0.341
32	2	0	27.09	0.06	40	20.27	0.288
33	2	0	26.17	0.06	50	20.41	0.302

shows that under low fly ash content, with the increase of fiber content, the peak and trough fluctuation of the PVA-ECC strain hardening zigzag section will become smaller. The value of b' is concentrated between 0.03 and 0.11. The dispersion of parameter b' is not as large as that of the four-stage multiple cracking sawtooth model parameter b', which means that at low fly ash content, with the increase of fiber content increase, the ratio of the increased stress to the ultimate tensile stress after uniaxial tension reaches the initial cracking stress of PVA-ECC is more stable. When the matrix material ratio is the same, the higher the fiber content, the more stable the strain-hardening section.

In the case of a particular matrix material mix ratio, the fiber increment increases the relative stress increment significantly, which is also in line with the macroscopic mechanical performance phenomenon. Under different fiber content, the initial cracking stress of the composite material does not change much. Because the matrix material mainly bears the stress in the linear elastic stage, the increase in fiber content significantly improves the tensile properties of the composite material, making the difference between the ultimate tensile stress and the initial cracking stress more considerable. In addition, limited data show that when the fiber content is constant and the other mixing ratios of the matrix materials remain unchanged, the effect of the increase in fly ash content on the relative stress increase is not apparent.

In the same set of experiments (data No. 16-23), the amount of fly ash can affect the model's parameters under

the same conditions as other mix ratios. The performance is that the higher the amount of fly ash, the larger the model parameters a and f values. That is the smaller the fluctuation of the sawtooth section, the more the number of sawtooth. Fly ash particles are primarily smooth and spherical, and other mixing ratios of the matrix material remain unchanged. Increasing the amount of fly ash can make the ECC material structure more uniform and improve the matrix–fiber interface transition zone. However, the increase in the amount of fly ash will reduce the matrix strength, so the initial cracking stress is reduced, and the matrix–fiber bonding force τ is reduced. When τ decreases, the proportion of fiber breakage during strain hardening decreases, the proportion of fiber withdrawal increases, and the proportion of fibers that are not broken or incompletely pulled out decreases.

For PVA-ECC, the applicable range of the three-stage multi-crack sawtooth model is as follows: the fiber content is more significant than 1.5%, and the fly ash content is not more than 10%. The higher the fiber content, the better the tensile properties of ECC. The fundamental reason is the increase in the number of fibers. When the ultimate bearing capacity is reached, the more fibers that bear the load, the better the tensile performance. The difference between the three-segment multiple cracking sawtooth model and the four-segment multiple cracking sawtooth model is that the amplitude of the ECC uniaxial tensile strain hardening section is stable, and there is no significant difference in saw tooth density and relative stress increment.

From the fitting of the four-stage multiple cracking model, it can be seen that in hardened section I, the proportion of fiber that is pulled off is more significant than the proportion of fiber pulled out, while in hardened section II, the proportion of fiber pulled off is smaller compared with ones pulled out. Under low fly ash content, when the fiber content reaches a particular critical value, such as PVA fiber content greater than 1.5%, during the ECC uniaxial tensile strain hardening process, the ratio of fiber breaking and pulling out is relative. It is stable so that the amplitude, increment, and density of the sawtooth in the entire strain hardening section are not apparent, so it is suitable for the three-segment multiple sawtooth models.

3.3 The effect of fiber reinforcement index on uniaxial tensile properties of PVA-ECC

Fiber Reinforcing Index $V_f \frac{L_f}{D_f}$ is another critical parameter in the theoretical fiber reinforcement system, related to the aspect ratio of the fiber and the fiber content. Five sets of PVA-ECC uniaxial tensile data with very similar matrix

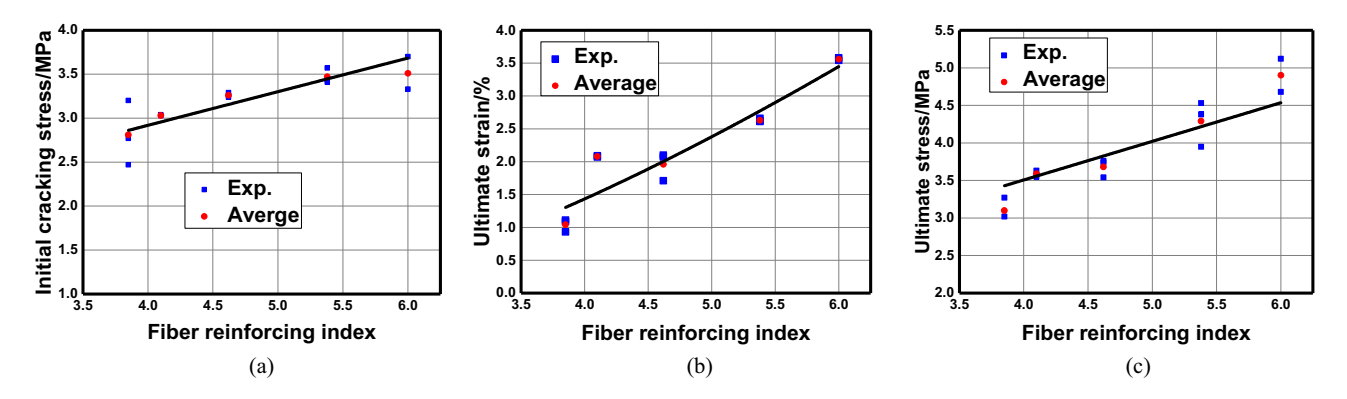


Figure 10: The relationship between uniaxial tensile properties of PVA-ECC and fiber reinforcement index: (a) initial cracking stress, (b) ultimate strain, and (c) ultimate stress.

materials and different fiber reinforcement indexes are used for data analysis, as shown in Figure 10.

Figure 10 shows the influence of the fiber-reinforcing index $V_{\rm f} \frac{L_{\rm f}}{D_{\rm f}}$ on the tensile properties of PVA-ECCs, which include $\sigma_{\rm fc}$, $\sigma_{\rm u}$, and $\varepsilon_{\rm u}$; increase with the fiber reinforcing index, and the relationship can be expressed by the following equations:

$$\sigma_{\rm fc} = 1.38887 + 0.38241 \times \frac{L_{\rm f}}{D_{\rm f}} V_{\rm f}, \qquad R^2 = 0.997, (21)$$

$$\sigma_{\rm u} = 1.45 + 0.51415 \times \frac{L_{\rm f}}{D_{\rm e}} V_{\rm f}, \qquad R^2 = 0.995,$$
 (22)

$$\varepsilon_{\rm u} = 0.01 + 2.13 \times F_{\rm I} - 2.54 \times \ln(F_{\rm I} + 1)$$

- 1.16 \times \ln^2(F_{\mathbf{I}} + 1), R^2 = 0.957. (23)

Using Eqs. (21), (22), and (23), inverse calculations are performed to convert the tensile properties accordingly and standard deviation and average standard deviation are obtained. The calculation results are shown in Table 3. It

can be seen from Table 3 that the average standard deviation of PVA-ECC tensile properties calculated using Eqs. (21) and (22) is low, the equation fitting effect is better, and the average standard deviation can be controlled within $\pm 6\%$.

3.4 Theoretical analysis of characteristic points of ECC uniaxial tensile stress-strain relationship based on experimental data

Studying the relationship between the initial cracking stress, initial cracking strain, ultimate tensile stress, and ultimate tensile strain of ECC uniaxial tension plays a vital role in the subsequent use of finite element software or self-edited software for ECC uniaxial tension simulation. Because these four mechanical properties indicate the starting and ending points of the multiple cracking stages in

Table 3: Conversion of PVA-ECC uniaxial tensile properties and relative error

No.	$V_{ m f} rac{L_{ m f}}{D_{ m f}}$	Initial cracking stress (MPa)	Converted initial cracking stress (MPa)	Ultimate stress (MPa)	Converted ultimate stress (MPa)	Ultimate strain (%)	Converted ultimate strain (%)
35–1 [53]	3.85	3.20	2.86(10.52%)	3.27	3.43(-4.74%)	1.11	1.30(-17.32%)
35-2	3.85	2.47	2.86(-15.59%)	3.02	3.43(-13.59%)	1.09	1.30(-19.09%)
35-3	3.85	2.77	2.86(-3.18%)	3.02	3.43(-13.67%)	0.93	1.30(-39.80%)
36-1 [59]	4.10	3.04	2.96(2.59%)	3.55	3.56(-0.13%)	2.07	1.52(29.60%)
36-2	4.10	3.03	2.96(2.34%)	3.63	3.56(1.87%)	2.09	1.52(29.60%)
37-1 [53]	4.62	3.24	3.15(2.67%)	3.54	3.82(-7.92%)	2.07	2.00(3.21%)
37-2	4.62	3.29	3.15(4.02%)	3.76	3.82(-1.62%)	2.10	2.00(4.77%)
37-3	4.62	3.26	3.15(-8.01%)	3.74	3.82(-2.12%)	1.71	2.00(-17.14%)
38-1 [53]	5.38	3.44	3.45(-0.35%)	3.95	4.22(-6.92%)	2.62	2.78(-19.68%)
38-2	5.38	3.41	3.45(-1.05%)	4.38	4.22(3.77%)	2.66	2.78(-8.58%)
38-3	5.38	3.57	3.45(3.32%)	4.53	4.22(6.80%)	2.61	2.78(-15.49%)
39-1 [56]	6.00	3.33	3.68(-10.73%)	4.68	4.53(3.08%)	3.54	3.45(2.56%)
39-2	6.00	3.70	3.68(0.46%)	5.12	4.53(11.37%)	3.58	3.45(3.67%)
Standard deviation			±4.99%		±5.97%		±16.20%

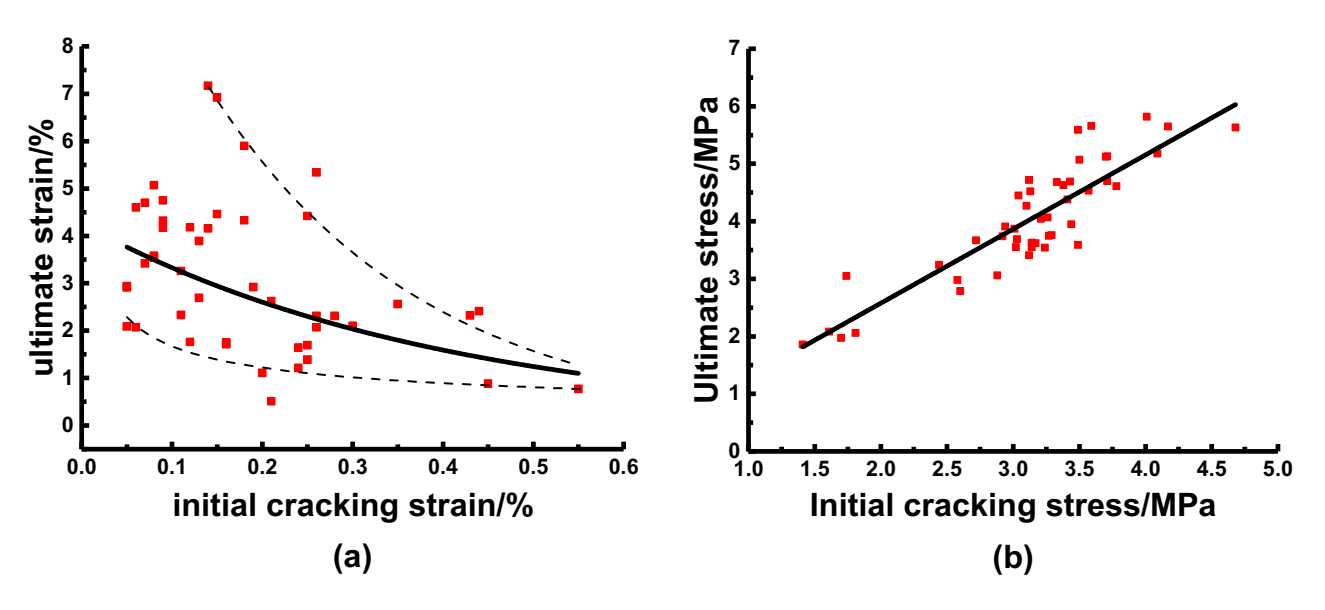


Figure 11: ECC uniaxial tensile stress-strain relationship characteristics: (a) limit stress – initial cracking stress, (b) limit strain – initial cracking strain.

the ECC uniaxial tensile stress–strain curve. Four mechanical properties of 46 sets of PVA-ECC uniaxial tensile specimens [16,53–58,60] were studied. The contents were the relationship between ultimate tensile strain and initial cracking strain and

the relationship between ultimate tensile stress and initial cracking stress (Figure 11).

Experimental data are shown in Table 4. The constitutive equations of PVA-ECC ultimate tensile stress—initial

Table 4: Uniaxial tensile properties of PVA-ECC

Data number	Initial cracking strength (MPa)	Initial cracking strain (%)	Ultimate strength (MPa)	Ultimate strain (%)	Data number	Initial cracking strength (MPa)	Initial cracking strain (%)	Ultimate strength (MPa)	Ultimate strain (%)
1 [53]	0.55	3.49	3.59	0.77	24 [54]	0.07	3.38	4.63	4.70
2	0.26	3.24	3.54	2.07	25	0.15	2.94	3.91	4.46
3	0.30	3.29	3.76	2.10	26	0.11	3.26	4.07	3.26
4	0.16	2.92	3.74	1.71	27 [55]	0.18	1.74	3.05	4.33
5	0.43	3.44	3.95	2.32	28	0.18	1.61	2.08	5.90
6	0.35	3.41	4.38	2.56	29	0.14	1.70	1.97	4.16
7	0.44	3.57	4.53	2.41	30	0.09	1.41	1.86	4.32
8	0.16	4.09	5.18	1.75	31 [60]	0.06	3.14	3.55	2.07
9	0.24	3.71	4.70	1.64	32	0.05	3.14	3.63	2.09
10	0.25	3.78	4.61	1.69	33	0.05	3.27	3.75	2.91
11	0.45	2.60	2.79	0.88	34 [16]	0.11	3.59	5.66	2.33
12	0.19	2.58	2.98	2.92	35	0.25	3.10	4.27	4.42
13	0.28	2.44	3.24	2.31	36	0.26	3.71	5.13	5.34
14	0.26	2.88	3.06	2.31	37	0.12	2.72	3.67	4.18
15	0.24	3.02	3.55	1.21	38	0.05	3.04	4.45	2.94
16	0.20	3.03	3.69	1.11	39 [57]	0.15	3.43	4.69	6.92
17	0.25	3.01	3.87	1.39	40	0.14	4.68	5.63	7.17
18	0.12	3.12	3.41	1.76	41 [58]	0.13	4.17	5.65	3.89
19	0.13	3.17	3.62	2.69	42	0.08	3.49	5.59	5.07
20	0.21	3.21	4.04	2.62	43	0.07	3.50	5.07	3.42
21	0.21	1.81	2.06	0.51	44	0.09	3.12	4.72	4.17
22 [56]	0.08	3.33	4.68	3.54	45	0.06	3.13	4.52	4.60
23	0.08	3.70	5.12	3.58	46	0.09	4.01	5.82	4.75

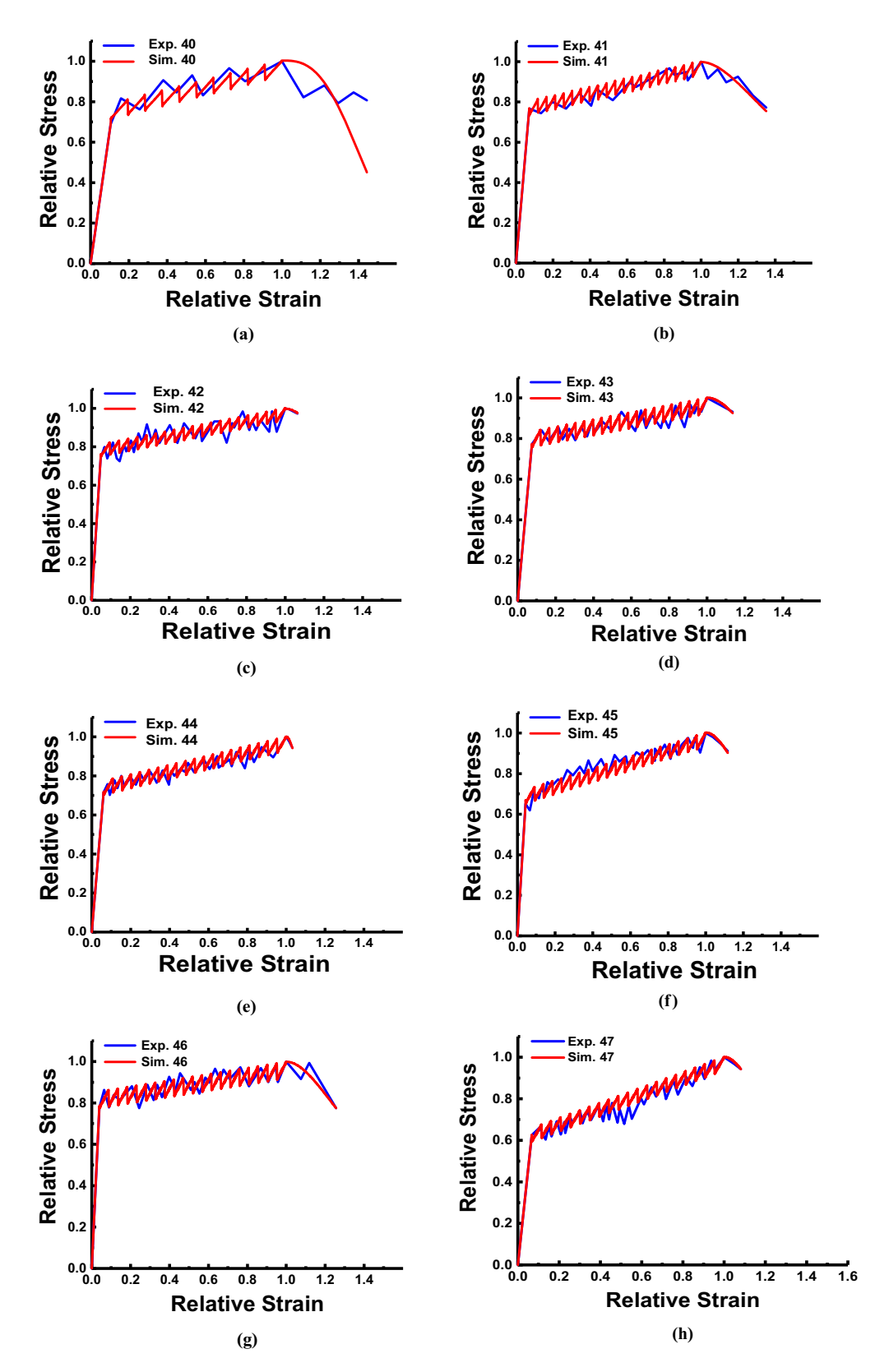


Figure 12: Curve fitting of PE-ECC three-segment multiple cracking sawtooth model: (a) 40, (b) 41, (c) 42, (d) 43, (e) 44, (f) 45, (g) 46, (h) 47, (i) 48, (j) 49, (k) 50, (l) 51, (m) 52, and (n) 53.

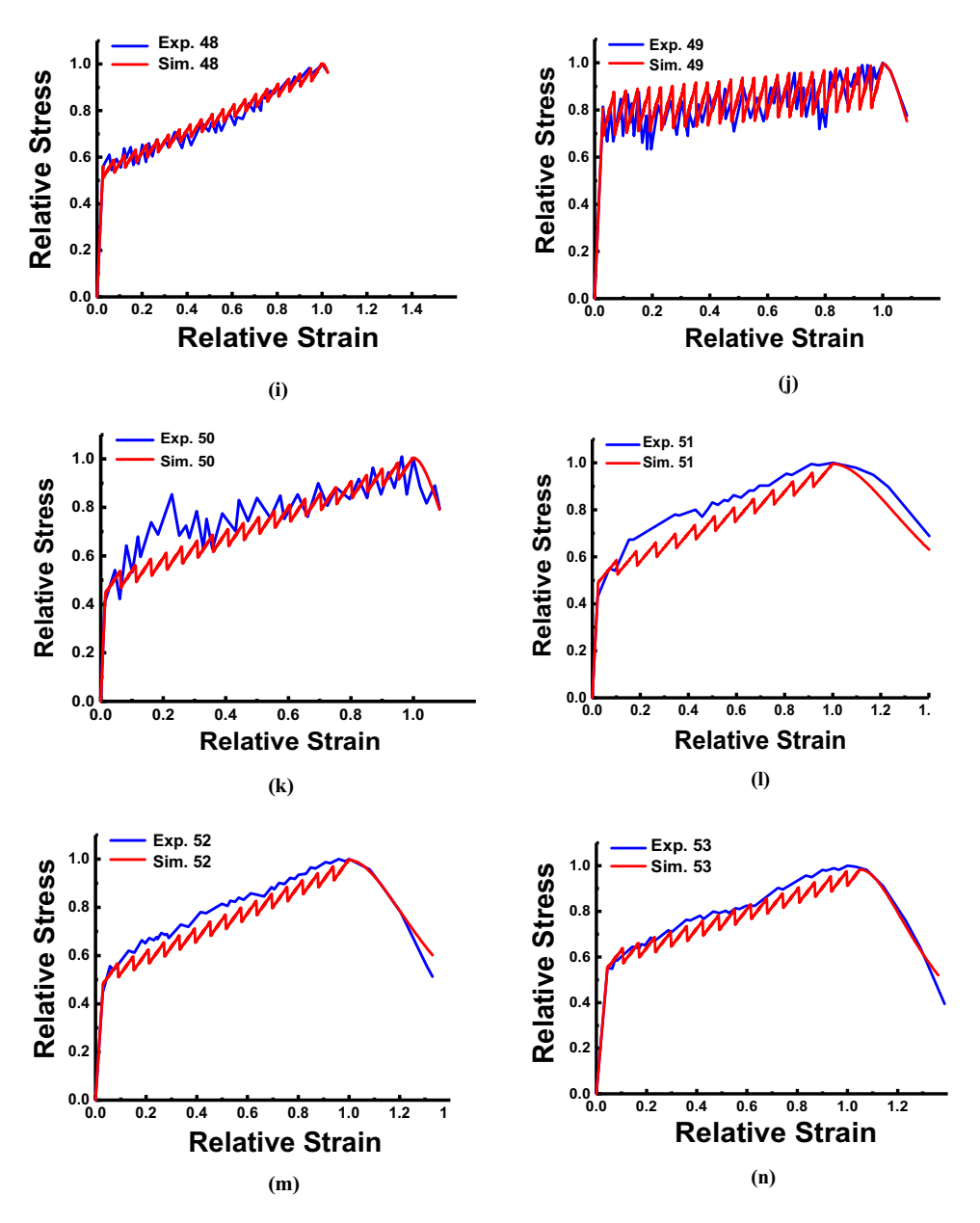


Figure 12: (Continued)

cracking stress and ultimate tensile strain—initial cracking strain are proposed:

$$\sigma_{\rm u} = 1.2887 \sigma_{\rm fc}, R^2 = 0.988 > R_{0.001}^2 = 0.216,$$
 (24)

$$\varepsilon_{\rm u} = 4.258e^{-2.462\varepsilon_{fc}}, R^2 = 0.25 > R_{0.001}^2 = 0.216.$$
 (25)

In the PVA-ECC uniaxial tensile test, the greater the initial cracking strain of the specimen, the smaller the ultimate tensile strain. The initial cracking strain of the specimen with a more considerable ultimate tensile strain is maintained at a low level, generally at most 0.2%. The ultimate tensile stress of PVA-ECC is linearly related to the initial cracking stress. The greater the initial cracking stress of the specimen, the greater the ultimate tensile stress.

4 PE-ECC uniaxial tensile stress-strain constitutive relationship

4.1 Three-segment multiple cracking sawtooth model fitting and parameter law

This article selects 11 groups of paper data [61–63] with similar mix ratios of matrix materials and different fiber content and fiber aspect ratios for model fitting. It is found that all data can be fitted by a three-stage multi-crack

Table 5: Fitting parameters	of PE-ECC uniaxial tensile three-st	tage multi-crack 'sawtooth' model

Data number	L _f (mm)	D _f (μm)	L _f /D _f	V _f (%)	a'	b'	с	f'	Δ
40 [61]	12	24	500	1.50	27.93	0.13	0.04	11.17	0.250
41	12	24	500	1.75	30.66	0.08	3.50	21.55	0.251
42	12	24	500	2	31.86	0.04	6.00	20.99	0.274
43	18	24	750	1.50	26.07	0.04	5.00	12.97	0.204
44	18	24	750	1.75	28.41	0.04	60.00	21.30	0.258
45	18	24	750	2	30.01	0.04	9.00	20.90	0.273
46	18	20	900	1.50	25.24	0.04	5.50	20.82	0.183
47	18	20	900	1.75	31.49	0.05	10.00	21.46	0.339
48	18	20	900	2	37.38	0.06	60.00	20.55	0.440
49 [62]	12	20	600	2	10.97	0.01	50.00	24.71	0.210
50	12	20	600	2	28.47	0.05	40.00	20.27	0.529
51 [63]	12.7	38	334	2	32.19	0.09	5.00	12.27	0.478
52	12.7	38	334	2	33.87	0.09	8.00	16.46	0.490
53	12.7	38	334	2	30.55	0.07	13.00	15.69	0.395

"sawtooth" model. Considering that the fiber content contains a mix ratio of not more than 1.5%, the f in the threestage model becomes adjustable. The fitting situation is shown in Figure 12:

The following conclusions can be drawn from Table 5 and Figure 13:

From Figure 13a and c, when the aspect ratio of PE fiber is constant, a' increases with the increase of fiber content. The smaller the fluctuation of the serrated section of the PE-ECC strain hardening section, the more stable the fluctuation section. The value of a' is concentrated between 25 and 33, which is more stable than the fitting parameter

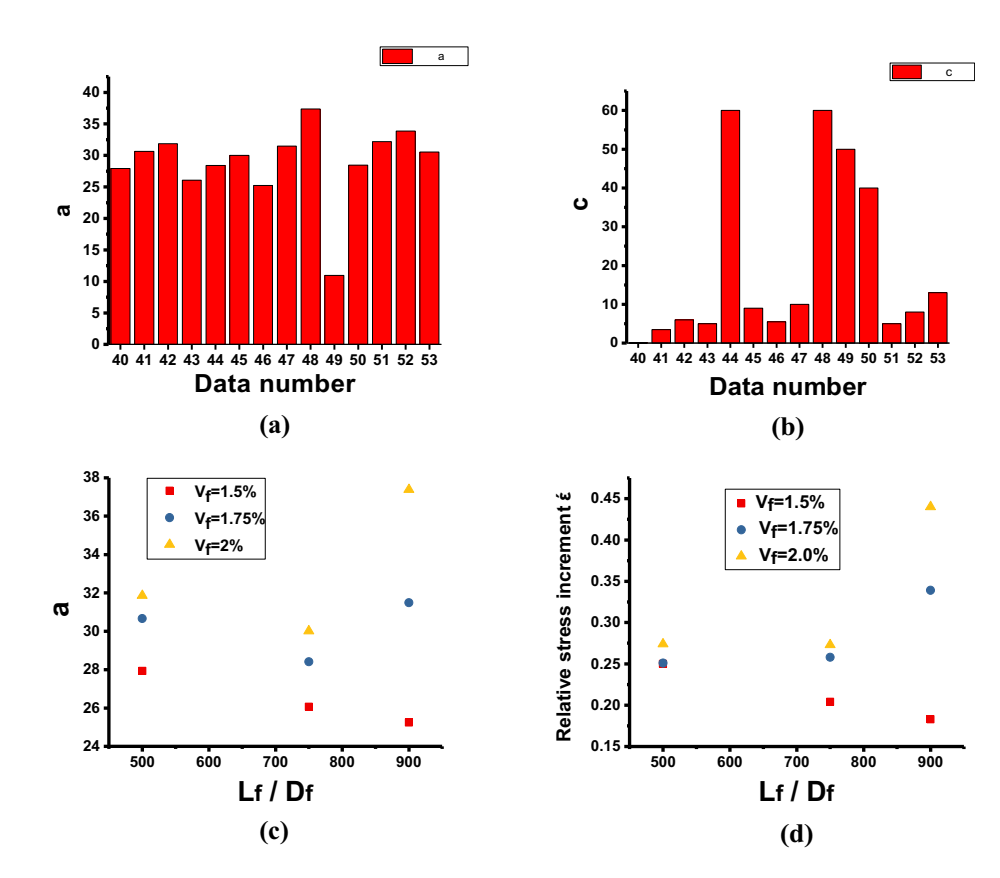


Figure 13: PE-ECC uniaxial tensile data fitting parameter distribution diagram: (a) the fitting parameter a of the model, (b) the fitting parameter c of the model, (c) relationship between fitting parameter a and fiber content, and (d) relationship between relative stress increment \triangle and fiber content.

Table 6: Physical and mechanical properties of PVA fiber and PE fiber

Fiber type	Length (mm)	Diameter (μm)	Density (g·cm ⁻³)	Elastic modulus (GPa)	Tensile strength (MPa)
PVA	8, 12	38-40	1.30	40-42.8	1,000–1,600
PE	12, 18	20, 24	0.97-0.98	100–120	2,700

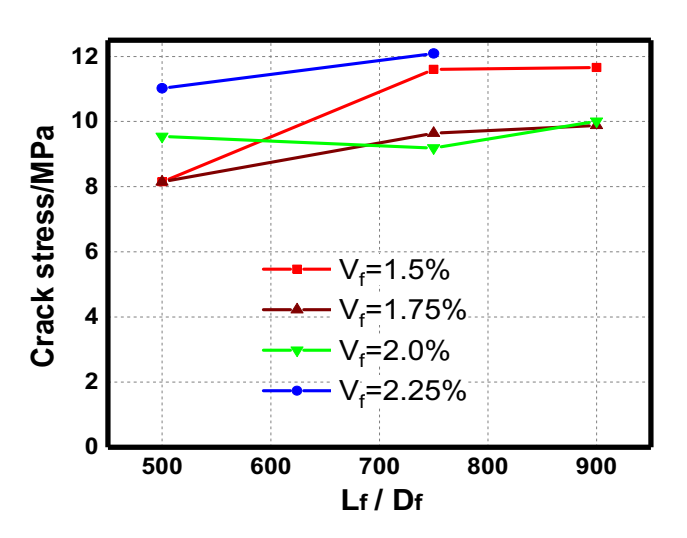
a' of the PVA-ECC three-stage multi-slit cracking "sawtooth" model.

The frequency f of the PE-ECC serrated segment is concentrated between 15 and 22, which is more stable than that of the PVA-ECC serrated segment, which is concentrated between 8 and 27.

From Tables 1 and 2, and Figure 13b, the strain softening segment parameter c in the uniaxial tensile stressstrain curve of PE-ECC is more minor, while the strain softening segment parameter c of PVA-ECC is more considerable, indicating that compared with PVA-ECC, PE-ECC has better ductility after reaching the strain softening point. PVA fiber has good hydrophilicity and interfacial bonding force between PVA fiber and cement matrix. The reason is that the non-circular and irregular cross-section of PVA fiber helps to expand the bonding surface between fiber and cement matrix. The molecular structure of PVA fiber is $(-CH_2-CHOH-)_n$, and its -C-OH group can form a strong hydrogen bridge with the -OH group in cement hydrate. The PE fiber is hydrophobic, which decreases the fibermatrix performance bond, and the fiber is not easy to break during the pull-out process.

In addition, the differences in physical and mechanical properties between PVA fiber and PE fiber are shown in Table 6.

It can be seen from Table 6 that the mechanical properties of PE fiber are better than those of PVA fiber, and the



DE GRUYTER

Figure 14: PE fiber aspect ratio and fiber content and PE-ECC uniaxial tensile initial crack stress diagram.

density of PE fiber is small. When the fiber volume content, fiber length, and fiber diameter are the same, the fiber number of PE fiber is more significant than that of PVA fiber. The ultimate bearing capacity of ECC depends on the number of fibers that have not quit the work at the maximum defect position and the tensile properties of the fibers. When the fiber volume content is the same, the tensile properties of PE-ECC are better than those of PVA-ECC.

Table 7: Fiber reinforcement index and PE-ECC uniaxial tensile performance index

Data number	L _f (mm)	D _f (μm)	L _f /D _f	V _f (%)	Fiber enhancement index	Initial cracking strength (MPa)	Ultimate tensile strength (MPa)	Ultimate tensile strain (%)
54 [61]	12	24	500	1.50	7.5	8.15	10.29	2.2
55	12	24	500	1.75	8.75	8.15	10.68	3.52
56	12	24	500	2	10	9.54	12.06	5.11
57	12	24	500	2.25	11.25	11.02	13.56	6.4
58	12	24	500	2.50	12.5	11.16	13.73	6.56
59	12	24	500	3	15	11.3	14.42	6.6
60	18	24	750	1.50	11.25	11.6	13.79	5.57
61	18	24	750	1.75	13.13	9.64	14.55	6.7
62	18	24	750	2	15	9.19	16.46	7.66
63	18	24	750	2.25	16.88	12.09	17.75	7.78
64	18	20	900	1.25	11.25	9.41	12.23	4.74
65	18	20	900	1.50	13.5	11.66	14.61	5.85
66	18	20	900	1.75	15.75	9.88	14.33	6.11
67	18	20	900	2	18	10.01	17.4	7.56

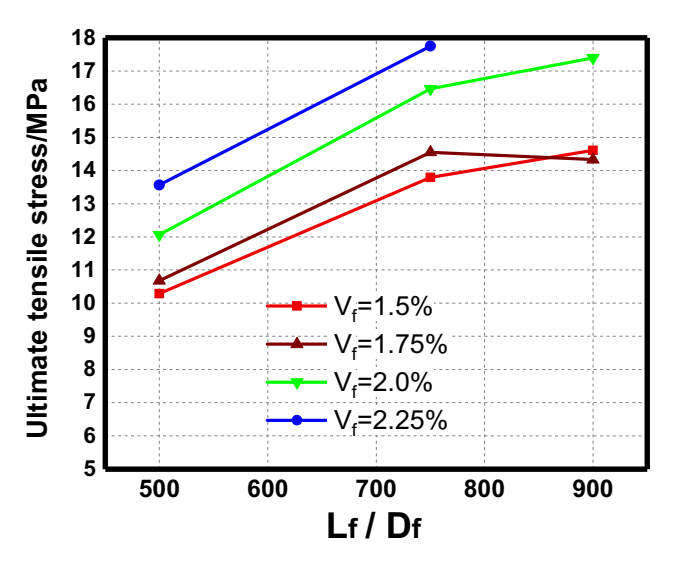


Figure 15: PE fiber aspect ratio and fiber content and PE-ECC uniaxial tensile ultimate tensile stress diagram.

From Figure 13d, when the aspect ratio of PE fiber is constant, the relative stress increment Δ increases with the increase in fiber content. The ratio of initial crack stress to ultimate tensile stress decreases.

4.2 The effects of aspect ratio and fiber reinforcement index on the uniaxial tensile properties of PE-ECC were studied

This articles selects 14 groups of paper data [61] with the same mix ratio of matrix materials and fiber content and

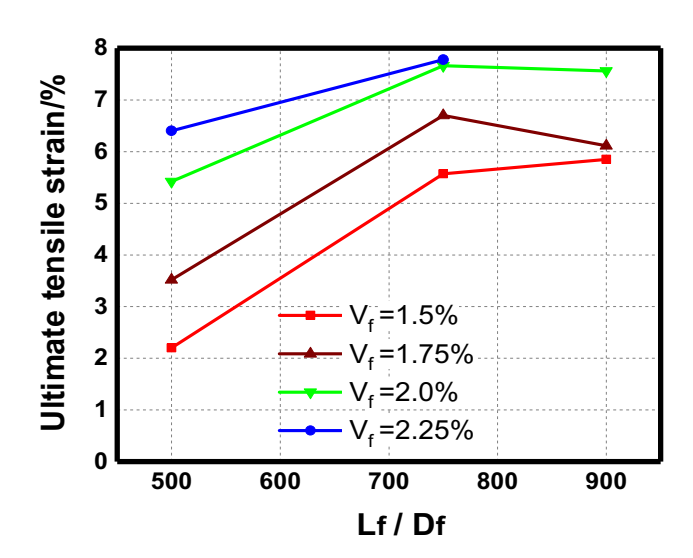


Figure 16: The relationship between the length–diameter ratio and fiber content of PE fiber and the ultimate tensile strain of PE-ECC under uniaxial tension.

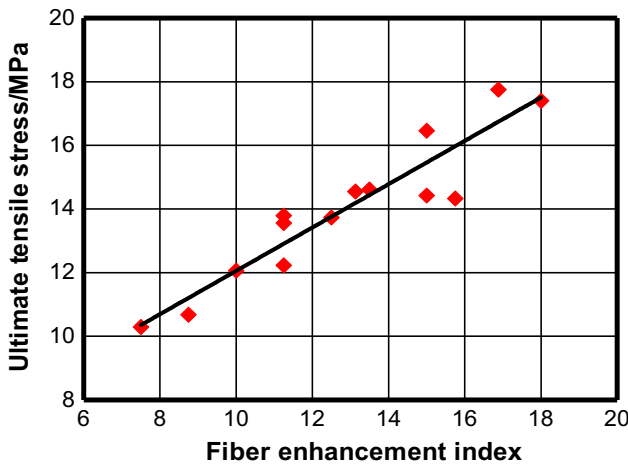


Figure 17: Relationship between ultimate tensile stress and PE fiber reinforcement index.

fiber aspect ratio for data analysis. The effects of different fiber reinforcement indexes on the initial crack strain, ultimate tensile stress, and ultimate tensile strain of PE-ECC uniaxial tension are analyzed, as shown in Table 7.

Figures 14–16 data show the influence of PE fiber aspect ratio and PE fiber content on the tensile properties of PE-ECC. When the fiber content increased from 1.5 to 2.0%, the ultimate tensile stress of PE-12-24, PE-18-24, and PE-18-20 increased by 17, 23 and 22%, respectively. Under the same fiber content (such as 2%), when the aspect ratio is 500,750 and 900, respectively, the peak stress is 12.06, 16.46, and 17.86 MPa, respectively; that is, the fiber aspect ratio increases by 50 and 80%, and the peak stress increases by 36 and 48%, respectively. The following conclusions can be drawn:

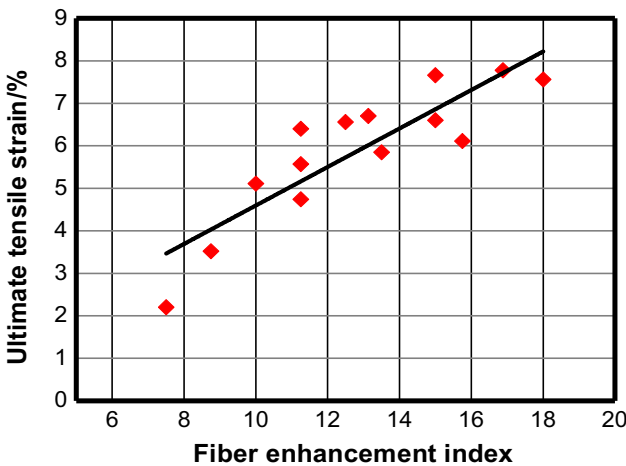


Figure 18: Relationship between ultimate tensile strain and PE fiber reinforcement index.

Table 8: PE-ECC conversion tensile properties a	d relative error
---	------------------

Data number	L _f /D _f	V _f (%)	Fiber enhancement index	Conversion ultimate tensile strength (MPa)	Relative error (%)	Conversion ultimate tensile strain (%)	Relative error (%)
1	500	1.50	7.5	10.35	-0.61	3.46	-57.49
2	500	1.75	8.75	11.20	-4.91	4.03	-14.51
3	500	2	10	12.06	0.03	4.60	15.24
4	500	2.25	11.25	12.91	4.81	5.16	19.33
5	500	2.50	12.5	13.76	-0.21	5.73	12.67
6	500	3	15	15.46	-7.22	6.86	-3.95
7	750	1.50	11.25	12.91	6.40	5.16	7.31
8	750	1.75	13.13	14.18	2.51	6.01	10.27
9	750	2	15	15.46	6.07	6.86	10.43
10	750	2.25	16.88	16.74	5.70	7.71	0.90
11	900	1.25	11.25	12.91	-5.54	5.16	-8.92
12	900	1.50	13.5	14.44	1.17	6.18	-5.67
13	900	1.75	15.75	15.97	-11.46	7.20	-17.85
14	900	2	18	17.50	-0.60	8.22	-8.72
Average	_	_	_	_	±4.09	_	±13.81

- 1) When the aspect ratio of PE fiber is constant, the initial crack stress, ultimate tensile stress, and ultimate tensile strain of PE-ECC increase with the increase of fiber content.
- 2) When the content of PE fiber is constant, the initial crack stress, ultimate tensile stress, and ultimate tensile strain of PE-ECC increase with the increase of aspect ratio.

The origin is used for data fitting, and the linear or ln function formula is used for fitting. The fitting situation is shown in Figures 17 and 18.

Based on the experimental data, the constitutive equations of the ultimate tensile stress—fiber reinforcement index and ultimate tensile strain—fiber reinforcement index are proposed:

$$\sigma_{\rm u} = 5.24522 + 0.68106 \times \frac{L_{\rm f}}{D_{\rm f}} V_{\rm f}, \ R^2 = 0.878,$$
 (26)

$$\varepsilon_{\rm u} = 0.06852 + 0.45283 \times \frac{L_{\rm f}}{D_{\rm f}} V_{\rm f}, \ R^2 = 0.767.$$
 (27)

Both formulas (26) and (27) are linear functions, and the intercepts of the two formulas represent the ultimate tensile stress and ultimate tensile strain of the matrix material without fiber incorporation, respectively. The matrix material used in the original article [61] is ultra-high-performance concrete (UHPC). It can be seen from the relevant research literature [64–66] that the intercept design of the constitutive equation is reasonable.

Using Eqs. (26) and (27) for inverse calculation, it is concluded that the corresponding tensile properties are calculated by fitting formula, and the relative error and average relative error are calculated. The calculation results are shown in Table 8.

It can be seen from Table 8 that the fitting formula is used to calculate the uniaxial tensile properties of PE-ECC inversely. The relative error of the converted ultimate tensile stress is $\pm 4.09\%$, and the relative error of the converted ultimate tensile strain is $\pm 13.81\%$.

5 Prospect of ECC strain hardening and multi-crack sawtooth constitutive model

This study proposes a multi-parameter ECC strain hardening and multi-crack sawtooth constitutive model. However, precise adjustment of parameters becomes especially critical when applying this model in practice. To further optimize the ECC model in subsequent research and deepen the understanding of the interactions between these parameters and their comprehensive impact on model performance, this section uses the data in Table 1 to perform Principal Component Analysis (PCA) on parameters such as $a_1', a_2', b_1', b_2', c', d, f_1', f_2', \Delta_{\text{II}}, \Delta_{\text{II}}$. The PCA results reveal the following key findings:

5.1 Variance explanation ratio

The goal of PCA is to reduce dimensions while capturing the most critical variability within the data. The analysis

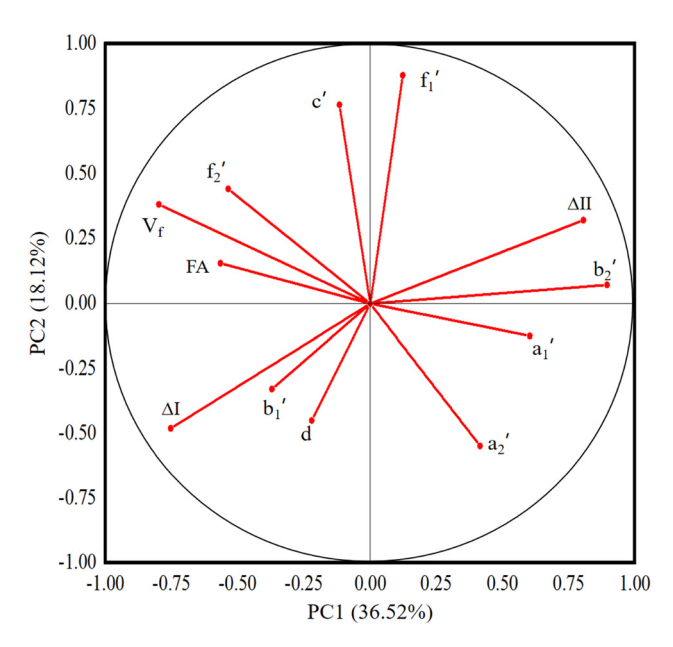


Figure 19: Correlation circle plot.

shows that the first principal component (PC1) explains 36.52% of the variance, indicating it captures the primary variability within the data. This suggests that PC1 may reflect the main response mechanism of ECC materials to strain hardening and multi-crack formation during the tensile process. For example, parameters strongly correlated with PC1 (such as b_2' , $\Delta_{\rm II}$, $\Delta_{\rm II}$) may be closely related to the material's crack propagation speed, crack width growth, or changes in crack spacing, which are key factors determining the material's toughness and ductility.

The second principal component (PC2) explains an additional 18.12% of the variance, providing further insights into the behavior of ECC materials, possibly related to changes in the microstructure of the material or the diversity of crack patterns.

5.2 Cumulative variance explanation

The first two principal components cumulatively explain 54.64% of the variance, while the first three explain 71.27%. This reveals complex but identifiable interaction patterns between model parameters. The increasing trend of cumulative variance explanation indicates that while single parameters may struggle to fully capture the complex behaviors of ECC materials, a comprehensive understanding of material responses can be effectively revealed by integrating the impacts of multiple parameters. Moreover, this suggests the existence of a core set of parameters within the material model that, when combined, can offer a holistic understanding of material behavior.

5.3 Principal component loadings and variable correlations

A more detailed analysis shows that PC1 is strongly positively correlated with b_2' , $\Delta_{\rm l}$, $\Delta_{\rm l}$, indicating these parameters play a pivotal role in the model. Figure 19 provides an intuitive way to understand the relationship between each variable and the principal components. For instance, the direction and length of vectors for parameters strongly correlated with PC1 (b_2' , $\Delta_{\rm l}$, $\Delta_{\rm ll}$) not only highlight the importance of these parameters for ECC material behavior but also reveal their relationships with other parameters in the material constitutive model. This visualization aids researchers in understanding which parameters are key when adjusting the model and how adjusting these parameters can improve the model's predictive accuracy and applicability.

This in-depth analysis also helps identify parameters that may require special attention in experimental design. For example, experiments that control these key parameters could more accurately verify the consistency between model predictions and actual observations, thereby optimizing model design.

In future research, these insights could be utilized to streamline the model by removing parameters that contribute less to the model's predictive capability. Such simplification can not only reduce computational costs but also enhance the model's applicability and universality. Additionally, further experimental data validation is needed to enhance the model's accuracy and robustness.

6 Conclusion

By collecting the literature data on ECC uniaxial tension, the law of its stress–strain curve was studied, and a new theoretical model of ECC uniaxial tension stress–strain constitutive relationship-multiple cracking sawtooth model was established.

Uniaxial tensile stress—strain curve for PVA-ECC is divided into two types: a four-segment multiple-cracking sawtooth model and a three-segment multiple-cracking sawtooth model. The four-segment multiple cracking sawtooth model is general. The relative stress increment of hardened section I is greater than that of hardened section II, and the sawtooth is denser. The applicable conditions of the three-segment multiple cracking sawtooth models are as follows: at low fly ash content, the PVA fiber content is more significant than 1.5%.

For the uniaxial tensile stress—strain curve of PE-ECC, only the three-stage multi-crack "sawtooth" model is used for fitting. The minimum content of PE fiber in the literature is 1.5%, and the stable single-hardening section can still be maintained. The fiber type has a significant effect on the mechanical behavior of ECC under uniaxial tension. When the matrix material and volume content are the same, the tensile properties of PE-ECC are better than those of PVA-ECC.

When the aspect ratio of PE fiber is constant, the initial crack stress, ultimate tensile stress and ultimate tensile strain of PE-ECC increase with the increase of fiber content. When the content of PE fiber is constant, the initial crack stress, ultimate tensile stress, and ultimate tensile strain of PE-ECC increase with the increase of aspect ratio.

The larger the fiber reinforcement index, the better the tensile performance of ECC. The fiber reinforcement index is linearly related to the initial crack stress and ultimate tensile stress of PVA-ECC, and the fiber reinforcement index is linearly related to the ultimate tensile stress and ultimate tensile strain of PE-ECC.

The characteristic points of PVA-ECC in the multi-slit cracking stage have the following laws: the greater the initial cracking strain, the smaller the ultimate tensile strain, which is exponentially related; the greater the initial cracking stress, the greater the ultimate tensile stress, which is linearly related.

Principal component analysis (PCA) was carried out on the parameters in Table 1, and the main parameters were found out, which provided a new method and new idea for the subsequent research of ECC strain hardening and multi-crack sawtooth constitutive model.

Funding information: The authors gratefully acknowledge the financial support of the Natural Science Foundation of China (Grant No. 52078250, 51508272).

Author contributions: Lingyu Li: writing, resources, methodology. Hongkang Chen: visualization, resources, analysis. Hongfa Yu: visualization, resources, analysis. Haiyan Ma: visualization, resources, analysis. Haotian Fan: data curation, accuracy. Xiaoqing Chen: investigation, data collection. Yuning Gao: visualization, resources, and analysis. All authors have accepted responsibility for the entire content of this manuscript and approved its submission.

Conflict of interest: The authors state no conflict of interest.

Data availability statement: The datasets generated and/ or analyzed during the current study are available from the corresponding author on reasonable request.

References

[1] Li, V. C. and C. K. Y. Leung. Steady state and multiple cracking of short random fiber composites. *Journal of Engineering Mechanics*, ASCE, Vol. 188, No. 11, 1992, pp. 2246–2264.

- [2] Li, V. C., From micromechanics to structural engineering-the design of cementitious composites for civil engineering applications, *JSCE Structure Mechanical and Earthquake Engineering*, Vol. 10, No. I–24, 1993, pp. 37–48.
- [3] Li, V. C., S. Wang, and C. Wu. Tensile strain-hardening behavior or polyvinyl alcohol engineered cementitious composite (PVA-ECC). ACI Materials, Vol. 98, No. 6, 2001, pp. 483–492.
- [4] Li, V. C. On engineered cementitious composites (ECC). A review of the material and its applications. *Journal of Advanced Concrete Technology*, Vol. 1, No. 3, 2003, pp. 215–230.
- [5] Li, V. C. Engineered cementitious composites (ECC) bendable concrete for sustainable and resilient infrastructure, Springer-Verlag GmbH, DE, part of Springer Nature, 2019.
- [6] Kong, H.-J., S. Bike, and V. C. Li. Development of a self-compacting engineered cementitious composite employing electrosteric dispersion/stabilization. *Cement & Concrete Composites*, Vol. 25, No. 3, 2003, pp. 301–309.
- [7] Fischer, G., S. Wang, and V. C. Li. Design of engineered cementitious composites (ECC) for processing and workability requirements. In *Proceedings, BMC-7*, Brandt, A. M., V. C. Li, and I. H. Marshall, eds, Woodhead Publishing, Warsaw, Poland, 2003, pp. 29–36.
- [8] Kim, Y. Y., H. J. Kong, and V. C. Li. Design of engineered cementitious composite (ECC) suitable for wet-mix shotcreting. ACI Materials Journal, Vol. 100, No. 6, 2003, pp. 511–518.
- [9] Kanda, T. and V. C. Li. Interface property and apparent strength of high-strength hydrophilic fiber in cement matrix. *Journal of Materials in Civil Engineering*, Vol. 10, No. 1, 1998, pp. 5–13.
- [10] Lepech, M. and V. C. C. Li. Preliminary findings on size effect In ECC structural members in flexure. *Brittle Matrix Composites*, Vol. 7, 2003, pp. 57–66.
- [11] Yu, K., L. Li, J. Yu, Y. Wang, J. Ye, and Q. F. Xu. Direct tensile properties of engineered cementitious composites: a review. Construction and Building Materials, Vol. 165, 2018, pp. 346–362.
- [12] Sahmaran, M., M. Li, and V. C. Li. Transport properties of engineered cementitious composites under chloride exposure. ACI Materials Journal, Vol. 104, No. 6, 2007, pp. 604–611.
- [13] Ranade, R., J. Zhang, J. P. Lynch, and V. C. Li. Influence of micro-cracking on the composite resistivity of engineered cementitious composites. *Cement and Concrete Research*, Vol. 58, 2014, pp. 1–12.
- [14] Liu, H., Q. Zhang, C. Gu, H. Su, and V. C. Li. Influence of microcracking on the permeability of engineered cementitious composites. *Cement & Concrete Composites*, Vol. 58, 2016, pp. 104–113.
- [15] Chen, Z., G. Zhang, and E.-H. Yang. Study of steel corrosion in strain-hardening cementitious composites (SHCC) via electrochemical techniques. *Electrochimica Acta*, Vol. 261, 2018, pp. 402–411.
- [16] Guo, L. P., B. Chen, W. Sun, and W. X. Zhang. Properties of high ductility cementitious composites for repair. *Journal of Building Structures*, Vol. 39, No. 7, 2018, pp. 169–174. (in Chinese).
- [17] Li, V. C. Durable overlay systems with engineered cementitious composites (ECC). *International Journal for Restoration of Buildings* and Monuments, Vol. 9, 2003, pp. 1–20.
- [18] Kojima Sakata, N., T. Kanda, and M. Hiraishi. Application of direct sprayed ECC for retrofitting dam structure surface-application for Mitaka-Dam. *In JCI Concrete Journal*, Vol. 42, No. 5, 2004, pp. 135–139.
- [19] Rokugo, K., M. Kunieda, and S. C. Lim. Patching repair with ECC on cracked concrete surface [A]. To appear in Proceeding. CONMAT 5 [C], 2005.
- [20] Li, V. C. and M. Lepech. Crack resistant concrete material for transportation construction [A]. *TRB 83rd Meeting [C]*, Washington, D C, CDROM, 2004, p. 4–4680.

- [21] Wang, S. and V. C. Li. Materials design of lightweight PVA-ECC [A]. In Proceedings of HPFRCC, Naaman A. E. and H. W. Reinhardt, eds, Ann Arbor MI, 2003, pp. 379-390.
- [22] Mechtcherine, V. Novel cement-based composites for the strengthening and repair of concrete structures. Construction and Building Materials, Vol. 41, 2013, pp. 365-373.
- [23] Müller, S., V. Mechtcherine, and M. Zydek. Behavior of strainhardening cement-based composites (SHCC) subject to cyclic loading. 7th International RELIM Workshop on High Performance Fiber Reinforced Cement Composites (HPFRCC), Stutggart, Germany, 2015.
- [24] Shen, B. Functionally graded fiber-reinforced cementitious composites - Manufacturing and extraction of cohesive fracture properties using finite elements and digital image correlation, Ph.D. University of Illinois at Urbana-Champaign, 2009.
- [25] Aveston, J. and A. Kelly. Theory of multiple fracture of fibrous composites. Materials Science, Vol. 8, No. 3, 1973, pp. 352-362.
- [26] Kabele, P. Multiscale framework for modeling of fracture in high performance fiber reinforced cementitious composites. Engineering Fracture Mechanics, Vol. 74, 2007, pp. 194-209.
- [27] Huang, T., Y. X. Zhang, and C. Yang. Multiscale modelling of multiple cracking tensile fracture behaviour of engineered cementitious composites. Engineering Fracture Mechanics, Vol. 160, 2016, pp. 52-66.
- [28] Li, J., J. Weng, and E. H. Yang. Stochastic model of tensile behavior of strain-hardening cementitious composites (SHCCs). Cement and Concrete Research, Vol. 124, 2019, id. 105856.
- [29] Luković, M., H. Dong, B. Šavija, E. Schlangen, G. Ye, and K. van Breugel. Tailoring strain hardening cementitious composite repair systems through numerical experimentation. Cement & Concrete Composites, Vol. 53, 2014, pp. 200-213.
- [30] Kang, J. and J. E. Bolander. Multiscale modeling of strain-hardening cementitious composites. Mechanics Research Communications, Vol. 78, 2016, pp. 47-54.
- [31] Shi, T. and C. K. Y. Leung. An effective discrete model for strain hardening cementitious composites: Model and concept.". Computers & structures, Vol. 185, 2017, pp. 27-46.
- [32] Kang, J. and J. Bolander. Event-based lattice modeling of strainhardening cementitious composites. International Journal of Fracture, Vol. 206, 2017, pp. 245-261.
- [33] Kabele, P. Stochastic fifinite element modeling of multiple cracking in fiber reinforced cementitious composites. In: Fracture and damage of advanced fibre-reinforced cement-red materials, Dresden, Germany, 2010, pp. 155-163.
- [34] Li, V. C. Performance driven design of fiber reinforced cementitious composites[C]. SWAMYRN. Proceedings of 4th RILEM International Symposium on Fiber Reinforced Concrete, E&FN Spon, London, 1992, p. 12-30.
- [35] Kanda, T., Z. Lin, and V. C. Li. Tensile stress-strain modeling of pseudo strain hardening cementitious composites. Journal of Mater in Civil Engineering, Vol. 12, No. 2, 2000, pp. 147-156.
- [36] Muhammer, K., F. Burak, and G. Eren. A comprehensive experimental study on the role of matrix structure on the multiple cracking behavior of PVA-ECC. Theoretical and Applied Fracture Mechanics, Vol. 121, 2022, id. 103503.
- [37] Tawfek, A. M., Z. Ge, H. Yuan, N. Zhang, H. Zhang, Y. Ling, et al. Influence of fiber orientation on the mechanical responses of engineering cementitious composite (ECC) under various loading conditions. Journal of Building Engineering, Vol. 63, No. Part B, 2023, id. 105518.

- [38] Do, T. D. D., K. J. Yen, C. H. Yen, and C. C. Hung. Impact of tension stiffening on the tensile and flexural behavior of ECC ferrocement. Construction and Building Materials, Vol. 329, 2022, id. 127201.
- [39] Mahmoudi, F., J. A. Abdalla, R. A. Hawileh, and Z. Zhang. Tensile and compressive strength of polyethylene engineered cementitious composite (PE-ECC) at elevated temperature. Materials Today: Proceedings, Vol. 65, No. Part 2, 2022, pp. 2081-2085.
- [40] Wu, J. D., L. P. Guo, X. P. Fei, B. C. Lyu, and B. Chen. Synergistic effects of silica fume and slag on the microstructure and mechanical behaviors of ultra-high-strength and high-ductility cementitious composites. Construction and Building Materials, Vol. 367, 2023, id. 130169.
- [41] Wu, J. D., L. P. Guo, B. Chen, B. C. Lyu, X. P. Fei, and R. S. Bian. Effect of PE fiber coated by polydopamine and nano-SiO₂ on the strain hardening behavior of ultra-high-strength and high-ductility cementitious composites. Cement and Concrete Composites, Vol. 136, 2023, id. 104852.
- [42] Zhang, Z., Y. Gao, F. Qin, F. Sun, and Y. Huang. Mechanical properties of sustainable high strength ECC with substitution of cement by limestone powder. Case Studies in Construction Materials, Vol. 19, 2023, id. e02434.
- [43] Teng, X., C. Lu, C. Li, and Z. Chen. Investigation on shear mechanical behavior of the interface between sulphoaluminate cement (SAC)-ECC and existing concrete, Vol. 403, 2023, id. 133184.
- Lai, B. L., M. Y. Zhang, Z. P. Chen, J. Y. R. Liew, and Y. Y. Zheng. Axial compressive behavior and design of semi-precast steel reinforced concrete composite columns with permanent ECC formwork. Structures, Vol. 57, 2023, id. 105130.
- [45] Pan, Z., Z. Qiao, D. Si, and J. Shang. Experimental investigation and numerical simulation on uniaxial tensile behavior of hybrid PVA-ECC. Construction and Building Materials, Vol. 398, 2023, id. 132517.
- Zhang, Z., J. Yu, F. Qin, Y. Huang, and F. Sun. Mechanical and selfhealing properties of calcium-sulfoaluminate-cement-based engineered cementitious composites (ECC). Journal of Building Engineering, Vol. 77, 2023, id. 107512.
- [47] Zhu, M., B. Chen, M. Wu, and J. Han. Energy evolution characteristics of engineered cementitious composites (ECC) under tensile and compressive loading. Journal of Building Engineering, Vol. 78, 2023, id. 107711.
- [48] Xiong, Y., K. Lin, D. Wu, Y. Ling, and S. Tesfamariam. The role of a novel coating of SFRCR-ECC in enhancing the fire performance of CFST columns: Development, characteristic and ISO-834 standard fire test. Engineering Structures, Vol. 294, 2023, id. 116629.
- [49] Wu, X., J. He, J. Tian, X. Tan, S. Hu, Y. Zheng, et al. Shear behaviors of engineered cementitious composites to seawater sea-sand concrete (ECC-to-SSSC) interfaces cast using 3D-printed pre-grooving formwork: Mechanical properties, characterization, and life-cycle assessment. Journal of Building Engineering, Vol. 78, 2023, id. 107636.
- [50] Liao, Q., Y. Su, J. Yu, and K. Yu. Torsional behavior of BFRP bars reinforced engineered cementitious composites beams without stirrup. Engineering Structures, Vol. 268, 2022, id. 114748.
- Zhou, W., W. McGee, H. S. Gökçe, and V. C. Li. A bio-inspired [51] solution to alleviate anisotropy of 3D printed engineered cementitious composites (3DP-ECC): Knitting/tilting filaments. Automation in Construction, Vol. 155, 2023, id. 105051.
- [52] Li, L., W. Liu, J. Wu, W. Wu, and M. Wu. Experimental investigation on the guasi-static tensile capacity of engineered cementitious composites reinforced with steel grid and fibers. Materials, Vol. 12, 2019, id. 2666.

- [53] Hao, H. Study of basic performance of injectable ultra-high toughnessstrength cementitious composite. [D], Nanjing. Southeast university, 2019.
- [54] Arce, G., H. Noorvand, M. Hassan, T. Rupnow, and R. Hungria. Costeffective ECC with low fiber content for pavement application[C]. MATEC Web of Conferences, Vol. 271, 2019, p. 07001.
- [55] Li, G., L. Huo, and T. Zhang. Uniaxial tensile properties of engineered cementitious composites. Materials Reports, Vol. 27, No. S1, 2013, pp. 298-301. (in Chinese).
- [56] Lee, B. Y., J. K. Kim, and Y. Y. Kim. Prediction of ECC tensile stressstrain curves based on modified fiber bridging relations considering fiber distribution characteristics. Computers and Concrete, Vol. 7, No. 5, 2010, pp. 455-468.
- [57] Xu, S. and X. Cai. Experimental study on mechanical properties of ultrahigh toughness fiber reinforced cementitious composite. Journal of Hydraulic Engineering, Vol. 40, No. 9, 2009, pp. 1055-1063. (in Chinese).
- [58] Xu, S. and H. Li. Uniaxial tensile experiments of engineered cementitious composites. China Civil Engineering Journal, Vol. 42, No. 9, 2009, pp. 32-41. (in Chinese).
- [59] Fischer, G., H. Stang, and L. Dick-Nielsen. Initiation and development of cracking in ECC materials: Experimental observations and modeling[C]. Proceedings of the 6th International Conference on Fracture Mechanics of Concrete and Concrete Structures, Vol. 3, 2007, pp. 1517-1522.

- [60] Dehghani, A., G. Fischer, and F. Alahi. Strengthening masonry infill panels using engineered cementitious composites. Materials and Structures, Vol. 48, No. 1-2, 2015, pp. 185-204.
- [61] Yu, K. Q., Z. D. Lu, J. G. Dai, and S. P. Shah. Direct tensile properties and stress-strain model of UHP-ECC. Journal of Materials in Civil Engineering, Vol. 32, No. 1, 2020, id. 04019334.
- [62] Wang, Y., M. Hou, J. Yu, S. Xu, K. Yu, and Z. Zhang. Experimental study on mechanical properties of ultra-high ductile cementitious composites. Material Guide B, Vol. 32, No. 20, 2018, pp. 3535-3540.
- [63] Li, V. C. Engineered cementitious composites (Ecc)-tailored composites through micromechanical modeling. Canadian Society for Civil Engineering, 1998, pp. 1-38.
- [64] Wu, P., M. Q. Sun, and Y. J. Wang. Study on tensile sensitivity of ultra high performance concrete. Bulletin of the Chinese Silicate Society, Vol. 38, No. 5, 2019, pp. 1331-1335 + 1342.
- [65] Shen, C., D. Tang, Z. Lyu, C. Yang, and L. Yu. Distribution of coarse aggregate and steel fibers in ultra-high performanceconcrete containing coarse aggregate (UHPC-CA) and their effect on the flexural performance. Construction and Building Materials, Vol. 421, 2024, id. 135666.
- [66] Zhang, Z., X. D. Shao, W. G. Li, P. Zhu, and H. Chen. Axial tensile behavior test of ultra high performance concrete. China Journal of Highway and Transport, Vol. 28, No. 8, 2015, pp. 50-58.